

# Uncertainty quantification in mechanistic epidemic models via cross-entropy approximate Bayesian computation

Americo Cunha Jr · David A. W. Barton · Thiago G. Ritto

Received: date / Accepted: date

**Abstract** This paper proposes a data-driven machine learning framework for parameter estimation and uncertainty quantification in epidemic models based on two key ingredients: (i) prior parameters learning via the cross-entropy method and (ii) update of the model calibration and uncertainty propagation through approximate Bayesian computation. The effectiveness of the new methodology is illustrated with the aid of actual data from COVID-19 epidemic at Rio de Janeiro city in Brazil, employing an ordinary differential equation-based model with a generalized SEIR-type mechanistic structure that includes time-dependent transmission rate, asymptomatics, and hospitalizations. A minimization problem with two cost terms (number of hospitalizations and deaths) is formulated, and twelve parameters are identified. The calibrated model provides a consistent description of the available data, able to extrapolate forecasts over a few weeks, which makes the proposed methodology very appealing for use in the context of real-time epidemic modeling.

A. Cunha Jr  
Rio de Janeiro State University – UERJ, Institute of Mathematics and Statistics, Rio de Janeiro, Brazil  
ORCID: 0000-0002-8342-0363  
E-mail: americo.cunha@uerj.br

D. A. W. Barton  
University of Bristol, Faculty of Engineering, Bristol, UK  
ORCID: 0000-0002-0595-4239  
E-mail: david.barton@bristol.ac.uk

T. G. Ritto  
Federal University of Rio de Janeiro – UFRJ, Department of Mechanical Engineering, Rio de Janeiro, Brazil  
ORCID: 0000-0003-0649-6919  
E-mail: tritto@mecanica.ufrj.br

**Keywords** COVID-19 modeling · machine learning · uncertainty quantification · cross-entropy method · ABC inference

## 1 Introduction

Since the COVID-2019 outbreak became a public information in January 2020 [73], many researchers have contributed with a variety of models to deal with this epidemic spread. They seek a better understanding of the disease's propagation mechanism and make short-term forecasts to guide public and private agents in related decision-making. In this context, mechanistic compartmental models with classical structures such as the SIR (susceptible, infected and removed), SEIR (susceptible, exposed, infected and removed) [2, 21, 69], or their variants with additional compartments [6, 7, 34, 35, 38] has been widely explored in literature.

These models are exciting tools to aid an epidemiologist since they can explain the past and explore future scenarios for an epidemic outbreak from qualitative and quantitative points of view. Thus they generate insight and can support decision making. Their balance between simplicity (fast to run simulations) and complexity (good to represent the phenomenology of the problem) may be an advantage for situations where analysis needs to be done in near-real-time (like in an evolving outbreak). Some examples of work in this direction are described below.

Pacheco et al. [41] analyzed an SEIR-type model and investigated different scenarios for Brazil. These authors highlight the importance of social isolation to avoid a collapse of the hospital infrastructure (in the early COVID-19 outbreak). Vyasarayani and Chatterjee [68] studied an SEIR model with an additional com-

partment for quarantine. They considered time delays for latency and an asymptomatic phase. Yu et al. [76] and Cai et al. [4] proposed a fractional versions of the SEIR model. None of the above investigations detail the calibration procedure or consider a stochastic model to propagate uncertainties.

On the other hand, Kucharski et al. [31] analyzed an SEIR model incorporating uncertainty in case observation. Using Poisson and binominal processes, these authors describe the dynamics of newly symptomatic cases, reported onsets of new infections, reported confirmation of cases, and the infection prevalence on evacuation flights. The calibration process is not detailed. He et al. [20] analyzed an SEIR model with hospitalization and quarantine. The model parameters are identified using the particle swarm optimization algorithm, a population-based stochastic optimization algorithm. Stochastic infection is considered by introducing a Gaussian white noise. Jha et al. [26] considered multiple coupled partial differential equations governing the evolution of susceptible, exposed, infectious, recovered, and deceased individuals. The Bayesian learning approach is implemented to calibrate the model parameters. They considered additive Gaussian noise to construct the likelihood function and assumed log-Normal priors. A different stochastic system is used by Lobato et al. [33], where a set of stochastic differential equations is employed to describe the random evolution of time-dependent parameters of a compartmental model.

For these models to be used in a customized way for the epidemic outbreak in a given geographic region, they need to be calibrated and validated with real (and reliable) data, in addition to, of course, quantifying the effects of random and epistemic uncertainties that arise in this context. An exciting methodology to identify the parameters of this type of highly nonlinear dynamic system is the cross-entropy (CE) method [11, 12, 13, 65, 70]. It is an iterative optimization procedure that starts with an initial probability density function for the parameters and updates it with data. In the limit of this process, the distribution converges to a degenerate measure (Dirac measure), which represents the optimal parameter values. On the other side, uncertainties play a major role in epidemiological models [54, 60]. Model parameters, the model structure itself, and the epidemic data are uncertain. Thus, beyond identifying parameters values, it is crucial to perform an uncertainty quantification (UQ) study, which can take into account the variability of the parameters. Probability theory might be used in this endeavor [8, 25, 56], and the Bayesian learning strategy [27, 53, 62] is convenient because prior knowledge is updated consistently with data and UQ occurs automatically. Approx-

imate Bayesian computation (ABC) is a likelihood-free strategy where the prior probability density function of the parameters is updated, with the aid of available data, only comparing the discrepancy between predictions and observations. It may be very useful in this setting since it can learn the parameter's joint distribution, propagate uncertainty throughout the model, and compute probabilistic envelopes of the response with a relatively low computational cost.

In this sense, this paper proposes a novel methodology for calibration and uncertainty quantification of a mechanistic epidemic model with two ingredients: (i) the cross-entropy method (CE) [9, 16, 29] to obtain a first estimation for the model parameters nominal values; (ii) approximate Bayesian computation (ABC) [64] to refine the estimation of the dynamic model parameters and describe the underlying parametric uncertainties. A two-step strategy is proposed where, first, the CE is employed to update the prior truncated Gaussian distribution that represents the uncertainties on the model parameters. ABC is then applied to refine the optimal parameter distributions and propagate the underlying uncertainties through the model. In comparison with other UQ strategies for epidemics available in the literature [20, 26, 31, 32, 33, 34, 77], the present methodology innovates by combining ABC and CE, resulting in a simple algorithm with theoretical guarantee of obtaining a good model calibration in typical situations. The effectiveness of the proposed methodology is illustrated with the aid of an SEIR-type epidemic model with seven compartments (susceptible, exposed, infectious, asymptomatic, hospitalized, recovered, and deceased) [42], and actual data from the city of Rio de Janeiro.

The paper is organized as follows. Section 2 depicts the mechanistic epidemic model. The proposed methodology that combines CE with ABC is presented in section 3. The results are shown in section 4. The manuscript body is closed with the concluding remarks in section 5.

## 2 SEIR(+AHD) epidemic model

### 2.1 Modeling of the contagion process

The compartmental model employed in this work to describe a COVID-19 outbreak in Rio de Janeiro city is schematically illustrated in Figure 1, where the population is segmented into seven disjoint compartments: susceptible (S); exposed (E); infectious (I); asymptomatic (A); hospitalized (H); recovered (R); deceased (D). This model is dubbed here as the SEIR(+AHD) model.

In this dynamic contagion model, the infection spreads via direct contact between a susceptible and an infected (infectious, asymptomatic, or hospitalized) individual. For simplicity, it is assumed that infectious and asymptomatic individuals are equally likely to transmit the disease to a susceptible person, while this risk is reduced in hospitalized individuals. The latency period between a person becoming infected, starting to have symptoms, and transmitting the disease, is taken into account by the presence of an exposed compartment, which counts those individuals who, despite carrying the pathogen, still do not show symptoms nor can infect other people. Among the infected, some individuals are asymptomatic; only a fraction display symptoms after incubation; they are dubbed infectious. Asymptomatic individuals can recover or die (a rare event). On the other hand, infectious individuals, in addition to recovery and death, may result in hospitalization. Hospitalized people reduce their probability of dying from the disease, but they can still have this outcome or recover. The recovered compartment is just an accumulator receiving individuals from various groups but does not directly interfere with the dynamics. This model was proposed by Pavack et al. [42], who were inspired by the age-structured model presented in [34], and its variant which considers ICU admissions presented in [40].

The population in each of the compartments at time  $t$  is measured by the following state variables: susceptible  $S(t)$ ; exposed  $E(t)$ ; infectious  $I(t)$ ; asymptomatic  $A(t)$ ; hospitalized  $H(t)$ ; recovered  $R(t)$ ; and deceased  $D(t)$ . Variable  $N = N(t)$  represents the alive population size at time  $t$ . This contagion model has the following parameters: initial alive population  $N_0$  (number of individuals); transmission rate  $\beta$  (days<sup>-1</sup>); latent rate  $\alpha$  (days<sup>-1</sup>); fraction of symptomatic  $f_E$  (non-dimensional); recovery rate  $\gamma$  (days<sup>-1</sup>); hospitalization rate  $\rho$  (days<sup>-1</sup>); death rate  $\delta$  (days<sup>-1</sup>); asymptomatic mortality-factor  $\kappa_A$  (non-dimensional); hospitalization mortality-factor  $\kappa_H$  (non-dimensional); and hospitalization infectivity-factor  $\epsilon_H$  (non-dimensional).

The deterministic non-autonomous dynamical system associated to this compartmental model (see [42]

for details) is written as

$$\begin{aligned}\dot{S} &= -\beta(t) S (I + A + \epsilon_H H)/N, \\ \dot{E} &= \beta(t) S (I + A + \epsilon_H H)/N - \alpha E, \\ \dot{I} &= f_E \alpha E - (\gamma + \rho + \delta) I, \\ \dot{R} &= \gamma (I + A + H), \\ \dot{A} &= (1 - f_E) \alpha E - (\kappa_A \delta + \gamma) A, \\ \dot{H} &= \rho I - (\gamma + \kappa_H \delta) H, \\ \dot{D} &= \delta (I + \kappa_A A + \kappa_H H), \\ \dot{N} &= -\dot{D},\end{aligned}\tag{1}$$

where the corresponding initial conditions are given by  $\mathbf{u}(0) = (S_0, E_0, I_0, A_0, H_0, R_0, D_0, N_0)$ . Obviously, if convenient, the size of this system can be reduced by one unit if the last equation is replaced by the algebraic constraint  $N = N_0 + D_0 - D$ , which represents the total population evolution over time.

## 2.2 Time dependence of the transmission rate

As the disease spreads, the parameter  $\beta$  might change, and this temporal dependence can be taken into account through the following expression (taken from [66]):

$$\beta(t) = \beta_0 + \frac{(\beta_\infty - \beta_0)}{2} \left( 1 + \tanh \left( \eta \frac{(t - t_\beta)}{2} \right) \right), \tag{2}$$

where  $\beta_0$  is the initial value of  $\beta$ ,  $\beta_\infty$  the final value, the adaptation time  $\eta$  defines how fast  $\beta$  reaches  $\beta_\infty$ , and  $t_\beta$  is the transition time (when  $t = t_\beta$  then  $\beta = (\beta_0 + \beta_\infty)/2$ ). This model allows  $\beta$  to smoothly vary between two distinct levels of disease transmission (from lower to higher, or vice versa), a situation typically encountered in the COVID-19 contagion dynamics [18,66].

## 2.3 Associated dynamic system

The dynamic state of the epidemic system (1) at time  $t$  can be represented, in a compact way, by the time-dependent vector

$$\mathbf{u}(t) = (S, E, I, A, H, R, D, N), \tag{3}$$

while the model parameters may be lumped into the parameter vector

$$\mathbf{x} = (\beta_0, \alpha, f_E, \gamma, \rho, \delta, \kappa_A, \kappa_H, \epsilon_H, \beta_\infty, \eta, t_\beta), \tag{4}$$

so that the dynamic model can be written as

$$\dot{\mathbf{u}}(t) = F(t, \mathbf{u}(t), \mathbf{x}), \tag{5}$$

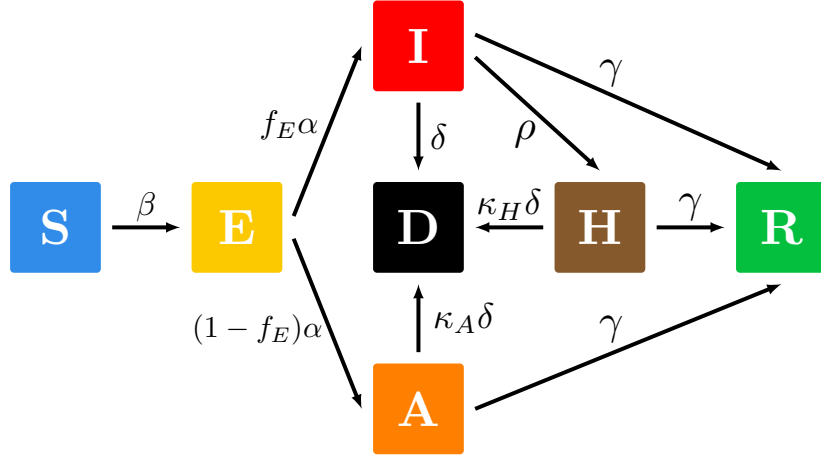


**Fig. 1** Schematic representation of the SEIR(+AHD) compartmental model considering latency period, asymptomatic individuals, hospitalizations, and deaths. This model is used here to describe the COVID-19 dynamics.

where the map  $(t, \mathbf{u}(t), \mathbf{x}) \mapsto F(t, \mathbf{u}(t), \mathbf{x}) \in \mathbb{R}^8$  represents the nonlinear evolution law defined by the right hand side of the dynamical system in (1).

#### 2.4 Applicability and limitations

The system of differential equations defined in (1) gives rise to a predictive computational model to describe the dynamics of COVID-19 contagion in a context where tracking the number of hospitalizations is essential.

Such a model can help study possible epidemiological scenarios and may lead to qualitative and quantitative insights into the epidemic dynamics. Such information can help guide decision-makers in managing their local health system. For instance, the model can check whether there is a risk of overloading the hospitals in a particular city. Also, they could estimate when they will suffer the most significant demand. From a more qualitative perspective, the model can assess the impact on hospitalizations of different strategies to mitigate (or even suppress) the epidemic.

But like any computational model, it is subject to limitations, and its use outside the proper context can lead to entirely erroneous predictions [63]. Since it is a deterministic compartmental model, obtained as a mean-field approximation in the thermodynamic limit, it is only applicable in regions where the population density can be modeled as a continuous function, a situation typically valid in urban centers of large cities. As it is a model derived from the SEIR family, it assumes a population with a homogeneous contact structure, which does not correspond to the reality of practically anywhere. Therefore, one must care about the potential effects of population heterogeneity.

Other unmodeled effects that may be significant are related to social behavior change due to the course of the epidemic (e.g. risk perception, change in the pattern of social interactions, mask use, etc.) [72], reinfections [46], etc. These can be included in the model, but this is not the goal of the present paper.

### 3 Uncertainty quantification framework

#### 3.1 Quantities of interest

Among all the quantitative information that can be estimated with the epidemic model in (1), this paper is particularly interested in two time-dependent quantities, the number of hospitalizations, and the total number of deaths, i.e., the quantities of interest here are the time series  $H(t)$  and  $D(t)$ .

None of these time series, individually or together, correspond to the response of the dynamic model itself. The model response is given by the parametric curve  $t \mapsto \mathbf{u}(t)$ , so that the above time series correspond to a derived quantity  $t \mapsto (H(t), D(t))$ , extracted from  $\mathbf{u}(t)$  through a projection.

On the theoretical plane,  $t \mapsto (H(t), D(t))$  is defined over a continuous-time domain and, consequently, is an infinite-dimensional object. However, for computational purposes, it is necessary to discretize both time-series so that, in practice, the dynamic model returns finite-dimensional representations of them. Once the computational representation of each time series materializes itself in the form of an  $n$ -dimensional numerical sequence, one might think that the model's discrete response is given by the quantities of interest vector

$$\mathbf{y} = [H(t_1), \dots, H(t_n), D(t_1), \dots, D(t_n)], \quad (6)$$

where  $t_1, \dots, t_n$  are the time-instants underlying the temporal discretization. If other observables become the quantities of interest, the vector  $\mathbf{y}$  can be modified straightforwardly. Just as if observables defined in different temporal grids are needed.

### 3.2 Abstraction of the epidemic model

In an abstract perspective, the computational model can be represented by an equation of form

$$\mathbf{y} = \mathcal{M}(\mathbf{x}), \quad (7)$$

which indicates that the vector  $\mathbf{y}$  is obtained from the vector of parameters  $\mathbf{x}$  through a mapping  $\mathcal{M}$ , which represents the discretized version of the dynamic model that is coded in the computer. Therefore, whenever convenient, the notation  $\mathbf{y}(\mathbf{x})$  is adopted.

Furthermore, if is necessary to distinguish the components of  $\mathbf{y}$  that are related to  $H(t)$  from those associated with  $D(t)$ , the following partition is adopted

$$\mathbf{y}(\mathbf{x}) = [\mathbf{y}^H(\mathbf{x}) \ \mathbf{y}^D(\mathbf{x})]. \quad (8)$$

In a case where there are  $K$  quantities of interest, the response vector is written

$$\mathbf{y}(\mathbf{x}) = [\mathbf{y}^1(\mathbf{x}) \ \dots \ \mathbf{y}^K(\mathbf{x})]. \quad (9)$$

This abstract representation helps to simplify the formulation of the uncertainty quantification framework presented in sequence.

### 3.3 Data from the epidemic surveillance system

Epidemiological surveillance data, represented in this paper by the vector quantity  $\mathbf{y}_{data}$ , can be used to monitor and understand (in real-time or a posterior) the course of an epidemic through direct observation, or in conjunction with computational models that can be calibrated and validated against them.

In this work, the data used are related to the records of hospitalizations and deaths due to COVID-19 in the city of Rio de Janeiro city, from Jan 01, 2020, until Dec 31, 2020. These data, shown in Figure 2, are cataloged and made available by local health authorities [44], being anonymous for ethical reasons and patient privacy.

For the sake of compatibility with the structure of  $\mathbf{y}(\mathbf{x})$ , the data vector  $\mathbf{y}_{data}$  which lumps hospitalizations and total deaths (or simply deaths) time series is partitioned as follows

$$\mathbf{y}_{data} = [\mathbf{y}_{data}^H \ \mathbf{y}_{data}^D]. \quad (10)$$

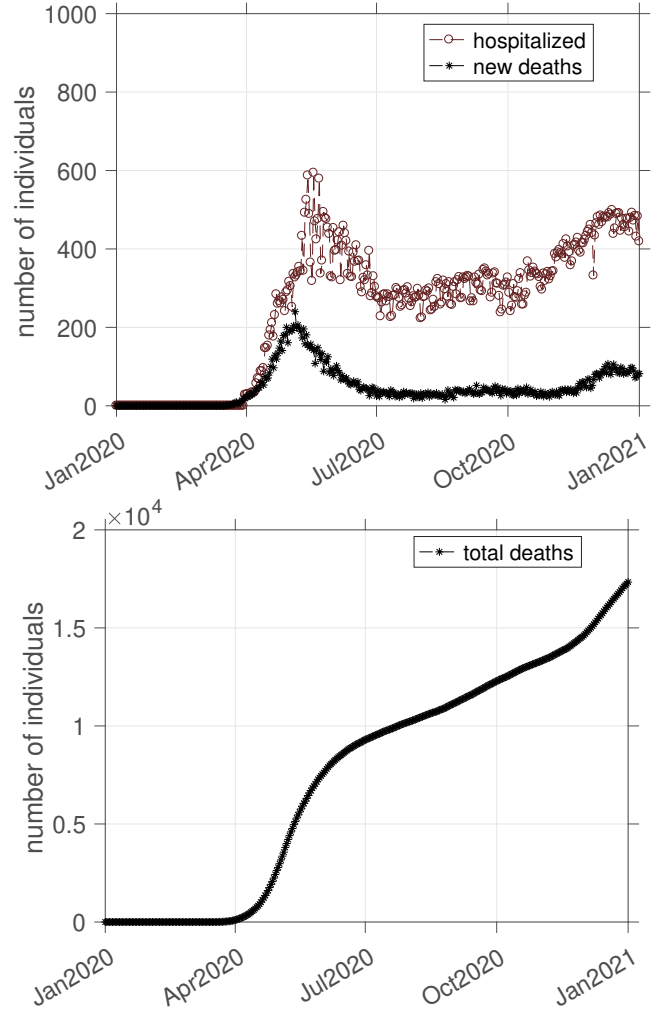


**Fig. 2** Surveillance data of COVID-19 outbreaks in Rio de Janeiro city between Jan 01, 2020, until Dec 31, 2020 [44]. The number of hospitalized individuals and new deaths appears at the top and the total number of deaths at the bottom.

A combination between these data and the epidemic model predictions is done in the uncertainty quantification framework presented below.

### 3.4 Quantification of the misfit between the mathematical model and available data

The comparison between data and predictions can be done by means of the following error estimation (misfit) function

$$\mathcal{J}(\mathbf{x}) = \omega \frac{\|\mathbf{y}_{data}^H - \mathbf{y}^H(\mathbf{x})\|^2}{\|\mathbf{y}_{data}^H\|^2} + (1 - \omega) \frac{\|\mathbf{y}_{data}^D - \mathbf{y}^D(\mathbf{x})\|^2}{\|\mathbf{y}_{data}^D\|^2}, \quad (11)$$

where  $\omega \in [0, 1]$  is a weight parameter which controls how the hospitalization/deaths data contributes to this

discrepancy function. For  $\omega = 0$ , only death data are taken into account. Conversely, for  $\omega = 1$  only hospitalization data matter. Between these extremes the error metric considers a balance between the two data sets. If  $\omega = 0.5$  they have the same weight. It is worth mentioning that we could identify  $\omega$  together with the other model parameters, including it in vector  $\mathbf{x}$ , possibility not explored in this paper.

In the case where  $K$  quantities of interest are available in the form of data, partitioned as

$$\mathbf{y}_{data} = [\mathbf{y}_{data}^1 \cdots \mathbf{y}_{data}^K], \quad (12)$$

so that the model response reads as in Eq.(9), and the misfit function is written as

$$\mathcal{J}(\mathbf{x}) = \sum_{k=1}^K \omega_k \frac{\|\mathbf{y}_{data}^k - \mathbf{y}^k(\mathbf{x})\|^2}{\|\mathbf{y}_{data}^k\|^2}, \quad (13)$$

with the weights defining a convex combination, i.e.,

$$\omega_1 + \cdots + \omega_K = 1. \quad (14)$$

### 3.5 Baseline calibration of model parameters via the Cross-Entropy (CE) method for optimization

The process of calibrating the computational model against the available data requires that the discrepancy function defined by Eq.(11) (or by Eq.(13)) be minimized by an optimal choice of parameters, a task that is mathematically formulated as the following optimization problem

$$\mathbf{x}^* = \arg \min_{\mathbf{x} \in \mathcal{X}} \mathcal{J}(\mathbf{x}), \quad (15)$$

where the set of admissible parameters is defined by

$$\mathcal{X} = \{ \mathbf{x} \mid \mathbf{x}_{min} \preceq \mathbf{x} \preceq \mathbf{x}_{max} \}, \quad (16)$$

where  $\mathbf{x}_{max}$  and  $\mathbf{x}_{min}$  represent, respectively, upper and lower bound vectors for the model parameters, and the generalized inequality  $\preceq$  is understood to hold for each component of the vectors.

In general, the optimization problem defined by (15) is nonconvex, so the use of gradient-based techniques may not be effective in capturing the parameter configuration that best fits the model to the data. Due to the nonconvexity, the solution obtained may be a local optimum (perhaps quite distinct from the global optimum). To avoid this type of situation, the present work tackles this optimization problem with the aid of the cross-entropy method [16, 48, 50], a simplistic gradient-free iterative procedure for global optimization that has guarantees of convergence in certain typical situations

[49, 50]. This method has been successfully used in recent literature for the identification of parameters in nonlinear computational models [11, 12, 13, 65, 70].

The fundamental idea of the cross-entropy method is to transform the optimization problem, defined by (15), into a rare event estimation problem. In this way, a sequence of approximations to the global optimum is constructed with the aid of an importance sampling process, where the probability of sampling the rare event (global optimum) grows over time [49, 50].

The CE algorithm consists of two phases:

- Sampling – where the objective function domain is sampled according to a certain distribution to explore the feasible region;
- Learning – where the distribution parameters are updated, with the aid of a set of elite samples. The goal is to shrink the distribution simultaneously as it is translated towards the global optimum.

To mathematically analyze the behavior of this algorithm, let  $\Gamma^* = J(\mathbf{x}^*)$  be the global minimum sought, and  $\mathbf{X}$  a randomized version of  $\mathbf{x}$ , with probability distribution characterized by the probability density function (PDF)  $p(\cdot, \mathbf{v})$ , i.e.,  $\mathbf{X} \sim p(\cdot, \mathbf{v})$ , for a parameter vector  $\mathbf{v} = (\boldsymbol{\mu}, \boldsymbol{\sigma})$ , with mean vector  $\boldsymbol{\mu}$  and standard deviation vector  $\boldsymbol{\sigma}$ .

Since  $\Gamma^*$  is the global optimal value of  $\mathcal{J}$ , there are few points  $\mathbf{x}$  in the domain  $\mathcal{X}$  that produce a value  $\Gamma = \mathcal{J}(\mathbf{x})$  very close to  $\Gamma^*$ , so that whenever  $\Gamma \approx \Gamma^*$ ,  $\mathcal{J}(\mathbf{x}) \leq \Gamma$  is a rare event, i.e.,

$$\mathcal{P}\{\mathcal{J}(\mathbf{x}) \leq \Gamma\} \approx 0 \text{ for } \Gamma \approx \Gamma^*. \quad (17)$$

The solution to this rare event estimation problem involves sampling the domain  $\mathcal{X}$  with  $N_{ce}$  samples – drawn according the distribution  $p(\cdot, \mathbf{v})$ , evaluate the objective function at the samples  $\mathbf{X}_k$ , and then construct of a sequence of estimators  $(\hat{\Gamma}_\ell, \hat{\mathbf{v}}_\ell)$  such that

$$\hat{\Gamma}_\ell \xrightarrow{a.s.} \Gamma^* \text{ and } p(\mathbf{x}, \hat{\mathbf{v}}_\ell) \xrightarrow{a.s.} \delta(\mathbf{x} - \mathbf{x}^*), \quad (18)$$

where the parameter vector  $\mathbf{v} = (\boldsymbol{\mu}, \boldsymbol{\sigma})$  is updated by solving the following nonlinear program

$$\hat{\mathbf{v}}_\ell = \arg \max_{\mathbf{v}} \sum_{k \in \mathcal{E}_\ell} \mathbf{1}\{\mathcal{J}(\mathbf{X}_k) \leq \hat{\Gamma}_\ell\} \ln p(\mathbf{X}_k; \mathbf{v}), \quad (19)$$

being  $\mathbf{1}\{\cdot\}$  the indicator function, and  $\mathcal{E}_\ell$  an elite sample set, defined by a fixed percentage of the samples  $\mathbf{X}_k$  that produced the values closest to the global optimum. Among the values associated with the elite set, the largest one defines the estimator  $\hat{\Gamma}_\ell$ .

The above sequence is optimal in the sense that the importance sampling process tries to minimize the

Kullback-Leibler divergence (also known as the cross-entropy function) between the sampling distribution  $p(\cdot; \mathbf{v})$  and a Dirac delta function centered on the global optimum [49, 50].

For sake of numerical implementation,  $p(\cdot, \mathbf{v})$  is assumed as a truncated Gaussian distribution with bounds defined in a conservative way. Distributions from the exponential family, like truncated Gaussian, allow the nonlinear program from Eq.(19) to be solved analytically [49, 50], so that the low-order statistics in the parameters vector  $\mathbf{v} = (\boldsymbol{\mu}, \boldsymbol{\sigma})$  are updated by simply calculating the sample mean and sample standard deviation from the elite sample set  $\mathcal{E}_\ell$ .

From a theoretical point of view, the process described above is guaranteed to converge to the global optimum [49, 50]. However, in practical terms, the distribution may degenerate before it gets close enough to this optimum point [29, 50]. To avoid this situation, the following smoothing scheme is employed

$$\hat{\boldsymbol{\mu}}_\ell := a \hat{\boldsymbol{\mu}}_\ell + (1 - a) \hat{\boldsymbol{\mu}}_{\ell-1}, \quad (20)$$

$$\hat{\boldsymbol{\sigma}}_\ell := b_\ell \hat{\boldsymbol{\sigma}}_\ell + (1 - b_\ell) \hat{\boldsymbol{\sigma}}_{\ell-1}, \quad (21)$$

$$b_\ell = b - b \left(1 - \frac{1}{\ell}\right)^q, \quad (22)$$

for a set of smooth parameters such that  $0 < a \leq 1$ ,  $0.8 \leq b \leq 0.99$  and  $5 \leq q \leq 10$  [29, 50], with the estimations at iterations  $\ell$  and  $\ell - 1$  obtained by solving the Eq.(19) analytically.

The convergence of the sampling process is controlled by the test

$$\|\boldsymbol{\sigma}_\ell - \boldsymbol{\sigma}_{\ell-1}\|_w \leq 1, \quad (23)$$

where the weighted root-mean-square norm of the difference vector  $\mathbf{x} - \mathbf{y} \in \mathbb{R}^N$  is defined as

$$\|\mathbf{x} - \mathbf{y}\|_w = \sqrt{\frac{1}{N} \sum_{j=1}^N (w_j (x_j - y_j))^2}, \quad (24)$$

for the error weights

$$w_j = \frac{1}{\text{atol}_j + 0.5 |x_j + y_j| \text{rtol}}, \quad (25)$$

with  $\text{atol}_j$  and  $\text{rtol}$  denoting absolute and relative tolerances, respectively. Due to the normalization provided by the weights of Eq.(25), a weighted norm of the order of 1 in (23) can be considered small. This type of convergence test, frequently used in the best differential equation solvers [22, 52], provides robust error control.

An overview of the cross-entropy method can be seen in Figure 3. More details about the CE implementation can be seen in Algorithm 1, section 3.7, and in the references [9, 49, 50].

### 3.6 Model update and uncertainty quantification through Approximate Bayesian Computation (ABC)

The update of the model calibration process involves a Bayesian inference scheme [27, 61], where the data set  $\mathbf{y}_{data}$  and a prior distribution for the parameters  $\pi(\mathbf{X})$  are combined with the aid of a likelihood function  $\pi(\mathbf{y}_{data} | \mathbf{X})$  to estimate a posterior parameter distribution  $\pi(\mathbf{X} | \mathbf{y}_{data})$  through Bayes' theorem

$$\pi(\mathbf{X} | \mathbf{y}_{data}) \propto \pi(\mathbf{y}_{data} | \mathbf{X}) \pi(\mathbf{X}), \quad (26)$$

which combines prior information and available data in an optimal way [61, 62].

For inference purposes in this setting, the approximate Bayesian computation (ABC) scheme proposed by Toni et al. [64] is employed. A likelihood function form is not assumed, so the usual hypothesis of additive independent Gaussian noise is unnecessary. Alternatively, the model prediction and the epidemic data are directly compared with the aid of a discrepancy function  $\mathcal{J}(\mathbf{x})$  — such as those defined by Eq.(11) or Eq.(13) — to measure the representation quality of the drawn model. Monte Carlo simulation [10, 29], employing an acceptance-rejection sampling strategy, is used in the inference process, in a way that a sample  $\mathbf{X}_k$  drawn from the prior distribution  $\pi(\mathbf{X})$  is accepted only if  $|\mathcal{J}(\mathbf{X}_k)| < \text{tol}$ , where  $\text{tol}$  is a (problem-dependent) tolerance prescribed by the user. Once the discrepancy function of Eq.(11) is defined as a kind of relative error, it is not necessary to employ two tolerances to control the convergence of the ABC process, as done in the case of CE. But the robust convergence criterion can be helpful for other definitions of  $\mathcal{J}(\mathbf{x})$ .

All known information about the model parameters should be encapsulated into a prior distribution  $\pi(\mathbf{X})$  to obtain an informative inference process. Typically, the iterative process of the CE method provides a lot of information about the parameters, so it is beneficial to take advantage of this knowledge to build the prior.

Therefore, the methodology proposed in this paper adopts as prior distribution, for the ABC inference step, the truncated Gaussian distribution with support bounds  $\mathbf{x}_{min}$ , and  $\mathbf{x}_{max}$ , central tendency  $\boldsymbol{\mu}$ , and dispersion information  $\boldsymbol{\sigma}$  that comes from the last iteration of CE algorithm, i.e.,

$$\pi(\mathbf{X}) = \mathcal{TN}(\boldsymbol{\mu}, \text{diag}(\boldsymbol{\sigma}), \mathbf{x}_{min}, \mathbf{x}_{max}). \quad (27)$$

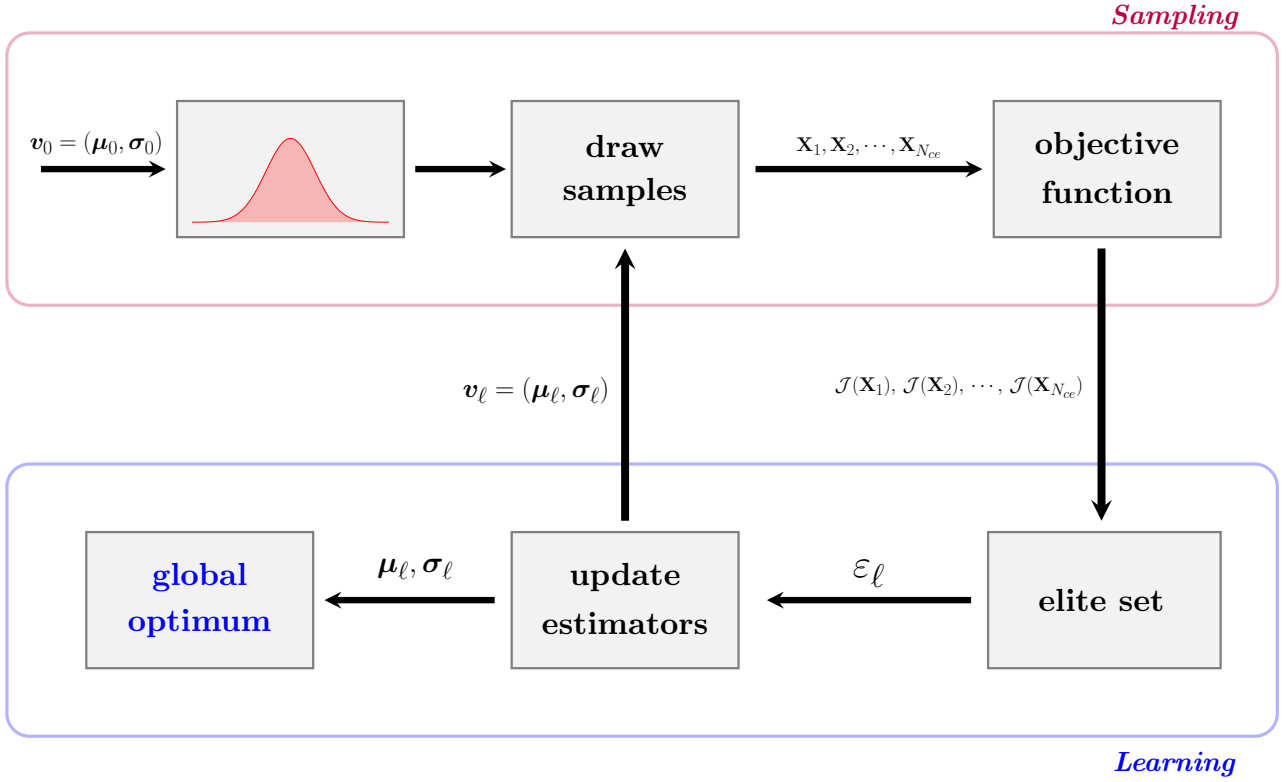


**Fig. 3** Schematic representation of the two-phases CE algorithm: (i) sampling – where the domain is sampled according to a given distribution to explore the feasible region, and (ii) learning – where the distribution parameters are updated with the aid of an elite set, to improve the optimum estimation.

It is important to note that although this prior distribution is defined in the same (broad) region where the initial truncated Gaussian of the CE method was defined, it is much more informative. Despite the support limits being kept invariant, the central tendency encapsulated in the mean  $\mu$ , and the dispersion defined by the standard deviation  $\sigma$  are updated by the CE iteration several times, obtaining a substantial gain of information in this process. Further details are available in Algorithm 1 from section 3.7.

Finally, it is also worth mentioning that the samples accepted in the rejection-sampling procedure, in addition to being used to characterize a posterior distribution of the parameters, are also used to calculate other statistical information for the model output, such as low-order moments, confidence bands, probabilities of interest, etc.

### 3.7 The novel metaheuristic CE-ABC framework for model calibration and uncertainty quantification

The combination of CE and ABC gives rise to a novel algorithm for model calibration (inversion) and uncertainty quantification (UQ). A schematic representation

of this new UQ framework, called here CE-ABC, can be seen in Figure 4.

First, a truncated Gaussian distribution, defined with aid of conservative bounds and informative values for central tendency, is used by CE method to sample the domain and obtain a first estimation for the model parameters values. After the convergence of this iterative process, the updated truncated Gaussian is used to define an informative prior distribution to be used in the ABC algorithm. The goal of the ABC is to combine prior information with data to obtain the posterior (informative) distribution of the parameters. A rejection-sampling algorithm is used to draw probabilistic envelopes. Other statistical information can be obtained in the same way. The computational recipe for the CE-ABC procedure is shown in Algorithm 1.

### 3.8 Remarks about the CE-ABC algorithm

The novel CE-ABC framework presented here is based on two general and well-established statistical methods, which have already been well studied in the specific literature and applied to several complex problems [50, 59, 64]. This combination results in an algorithm that



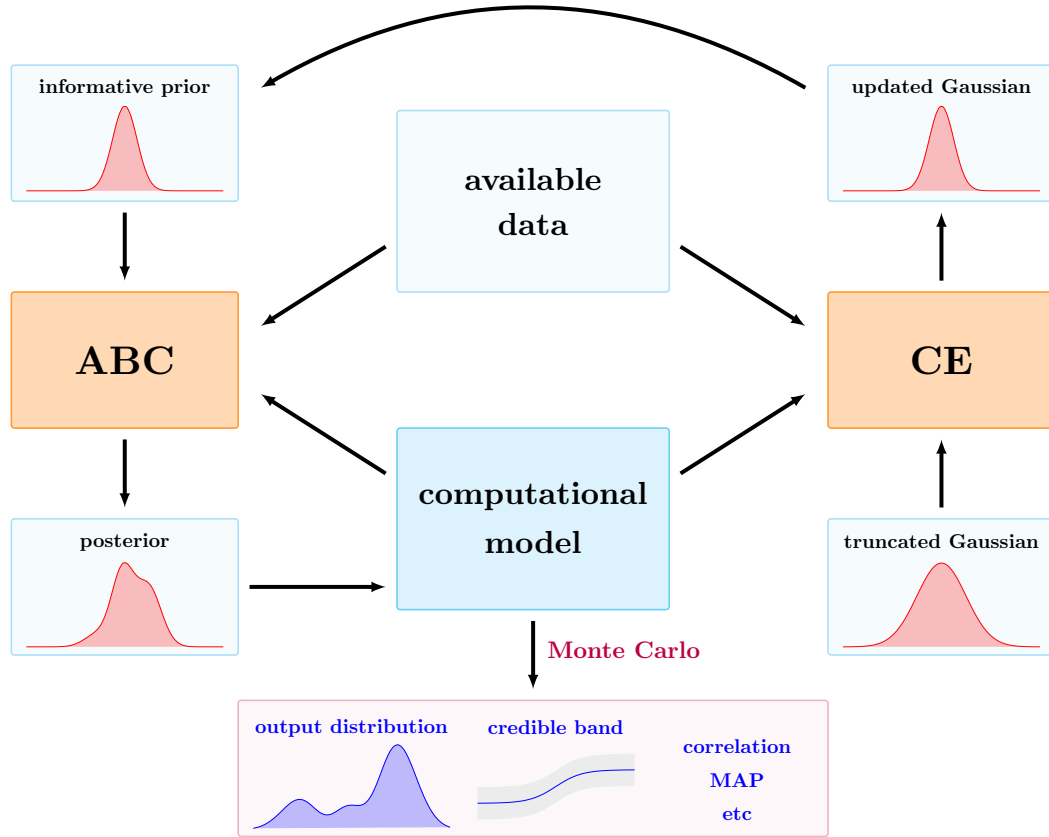


**Fig. 4** Schematic representation of the CE-ABC framework for estimating parameters and uncertainty quantification. First, an estimate for the model parameters is obtained with the cross-entropy (CE) method. Then, the estimation of the parameters is refined through an inference process employing approximate Bayesian computation (ABC), which also propagates the uncertainties through rejection-sampling Monte Carlo simulation.

inherits the good properties of both methods: (i) guarantee of convergence to the global optimum by the CE; and (ii) independence of likelihood and relatively low<sup>1</sup> computational cost due to ABC. Such a mixture of good properties generates a robust framework for simulations involving mechanistic epidemic models, which are typically difficult to calibrate and have a limited predictability horizon, requiring quantification of uncertainties for any minimally reliable forecast.

Although the good theoretical properties of the CE-ABC framework are observed in the numerical studies developed by the authors with the epidemic model employed in this paper, its use in conjunction with other types of computational models requires a more comprehensive theoretical analysis. Such a formal analysis for a broad class of models is beyond the scope of this work and the present journal, but it would be a fascinating work on applied mathematics, which the authors leave as a suggestion for future work.

<sup>1</sup> The mechanistic epidemic models used here can be integrated into a fraction of a second so that the CE-ABC simulation takes only a few minutes, a relatively low cost.

In this way, due to the generality of CE and ABC methods, but in a context where a rigorous mathematical analysis to ensure algorithm functionality for a broad class of computational models is missing, the proposed CE-ABC framework can be considered a meta-heuristic for model calibration and UQ.

Despite the CE-ABC algorithm's excellent convergence properties, it is impossible to make an accurate inference if “bad” values (physically/biologically inconsistent or very discrepant with reality) are assigned to the model's nominal parameters, initial conditions, and bounds. Defining the bounds and nominal values for the parameters and initial conditions is an important task that must be done carefully. It is necessary to know in depth the problem of interest. The analyst's experience with the problem of interest is essential; it is a kind of expert knowledge that must be embedded into the priors distributions. Besides, exploratory tests with the computational model and information from previous works may be precious to discover a suitable interval of values.

**Algorithm 1** CE-ABC is a metaheuristic that combines CE and ABC for parameters estimation and uncertainty quantification in mechanistic epidemic models. It receives as input the computational  $\mathcal{M}$ , the misfit function  $\mathcal{J}$ , the sampling distributions bounds  $\mathbf{x}_{min}$  and  $\mathbf{x}_{max}$ , the number of CE samples  $N_{ce}$ , the elite sample set size  $N_{\mathcal{E}_\ell}$ , the number of ABC samples  $N_{abc}$ , an absolute and a relative tolerance for CE **atol** and **rtol**, a tolerance for ABC **tol**, and an upper bound for CE iterations **maxiter**. The algorithm returns the best parameter estimate obtained by both CE and ABC, and the samples accepted during the ABC iteration process.

---

```

1: procedure CE-ABC( $\mathcal{M}, \mathcal{J}, \mathbf{x}_{min}, \mathbf{x}_{max}, N_{ce}, N_{\mathcal{E}_\ell}, N_{abc}, \text{atol}, \text{rtol}, \text{tol}, \text{maxiter}$ )

```

```

Require:  $\mathbf{x}_{min} \preceq \mathbf{x}_{max}$ 

```

```

Require:  $N_{ce} > 0$ 

```

```

Require:  $N_{abc} > 0$ 

```

```

Require:  $N_{\mathcal{E}_\ell} > 0$  and  $N_{\mathcal{E}_\ell} < N_{ce}$ 

```

```

Require:  $\text{atol} \geq 0$ 

```

```

Require:  $\text{rtol} > 0$ 

```

```

Require:  $\text{tol} > 0$ 

```

```

Require:  $\text{maxiter} > 0$ 

```

```

    //----- CE step -----//
2:  $\ell := 0$ 
3:  $\boldsymbol{\mu} := (\mathbf{x}_{max} + \mathbf{x}_{min})/2$ 
4:  $\boldsymbol{\sigma} := (\mathbf{x}_{max} - \mathbf{x}_{min})/\sqrt{12}$ 
5: Draw  $\mathbf{X} \sim \mathcal{TN}(\boldsymbol{\mu}, \text{diag}(\boldsymbol{\sigma}), \mathbf{x}_{min}, \mathbf{x}_{max})$  // total of  $N_{ce}$  samples
6: while  $\|\boldsymbol{\sigma}_\ell - \boldsymbol{\sigma}_{\ell-1}\|_w > 1$  and  $\ell < \text{maxiter}$  do
7:    $\ell := \ell + 1$ 
8:   Evaluate  $\mathbf{Y}_k = \mathcal{M}(\mathbf{X}_k)$  for  $k = 1 : N_{ce}$ 
9:   Evaluate  $\mathcal{J}(\mathbf{X}_k)$  for  $k = 1 : N_{ce}$ 
10:   Define elite sample set  $\mathcal{E}_\ell$ 
11:   Update  $\boldsymbol{\mu}$  and  $\boldsymbol{\sigma}$  using  $N_{\mathcal{E}_\ell}$  samples from  $\mathcal{E}_\ell$ 
12: end while
    //----- ABC step -----//
13:  $\mathcal{J}_{min} = \infty$ 
14:  $\mathbf{X}_{best} = \text{NaN}$ 
15:  $\mathbf{Y}_{best} = \text{NaN}$ 
16: Define prior  $\pi(\mathbf{X}) = \mathcal{TN}(\boldsymbol{\mu}, \text{diag}(\boldsymbol{\sigma}), \mathbf{x}_{min}, \mathbf{x}_{max})$ 
17: Draw  $\mathbf{X} \sim \pi(\mathbf{X})$  // total of  $N_{abc}$  samples
18: for  $k = 1 : N_{abc}$  do
19:   Evaluate  $\mathbf{Y}_k = \mathcal{M}(\mathbf{X}_k)$ 
20:   Evaluate  $\mathcal{J}(\mathbf{X}_k)$ 
21:   if  $\mathcal{J}(\mathbf{X}_k) < \text{tol}$  then
22:     Accept  $\mathbf{X}_k$ 
23:     Save  $\mathbf{X}_k$  and  $\mathbf{Y}_k$ 
24:     if  $\mathcal{J}(\mathbf{X}_k) < \mathcal{J}_{min}$  then
25:        $\mathbf{X}_{best} := \mathbf{X}_k$ 
26:        $\mathbf{Y}_{best} := \mathbf{Y}_k$ 
27:        $\mathcal{J}_{min} := \mathcal{J}(\mathbf{X}_k)$ 
28:     end if
29:   else
30:     Reject  $\mathbf{X}_k$ 
31:   end if
32: end for
33: Return  $(\mathbf{X}, \mathbf{Y})_{opt}^{ce}$ ,  $(\mathbf{X}, \mathbf{Y})_{best}^{abc}$ , and  $(\mathbf{X}, \mathbf{Y})_{saved}^{abc}$ 
34: end procedure

```

---

The results obtained with the CE-ABC framework also strongly depend on the tolerances **atol**, **rtol**, and **tol**, chosen by the user. There are no canonical values for these parameters that are valid for all types of inference; good values are problem-dependent. In this way, the analyst's experience and intuition are crucial in defining these values and a little numerical experimentation with the model with the computational model. In the numerical experiments repeated in the session 4

these tolerances are defined as being **atol** = 0.001, **rtol** = 0.05, and **tol** = 0.1.

Once again, it is worth emphasizing the observations made in section 2.4 about the limitations and applicability of the model. No matter how robust the calibration and uncertainty propagation algorithm is, how good is the choice of model parameters and bounds. If the model does not describe the interest situation in a minimally reliable way, terribly wrong (or in the limit nonsense) predictions will emerge from the simulations.

**Table 1** Plausible nominal values and bounds for the parameters of the SEIR(+AHD) epidemic model.

|                      | Unit  | Nominal | Min    | Max   | Refs         |
|----------------------|-------|---------|--------|-------|--------------|
| $\beta$ or $\beta_0$ | 1/day | 1/7     | 1/10   | 1/2   | [36, 74]     |
| $\alpha$             | 1/day | 1/5     | 1/10   | 1/2   | [5, 36]      |
| $f_E$                | —     | 0.8     | 0.7    | 0.9   | [3, 36, 39]  |
| $\gamma$             | 1/day | 1/14    | 1/21   | 1/7   | [36, 78]     |
| $\rho$               | 1/day | 1/1000  | 1/3500 | 1/800 | [36, 71, 78] |
| $\delta$             | 1/day | 1/5000  | 1/8000 | 1/100 | [57]         |
| $\kappa_A$           | —     | 0.001   | 0.0005 | 0.005 | —            |
| $\kappa_H$           | —     | 0.05    | 0.01   | 0.1   | [19, 36, 74] |
| $\epsilon_H$         | —     | 0.2     | 0.1    | 0.5   | —            |
| $\beta_\infty$       | 1/day | 1/4     | 1/10   | 1/2   | [66]         |
| $\eta$               | 1/day | 1       | 0      | 2     | [66]         |
| $\tau_\beta$         | day   | 60      | 0      | 120   | [44]         |

Choosing a suitable model is a primary exercise and of great importance in this type of analysis.

## 4 Results and discussion

This section presents several numerical experiments conducted with the SEIR(+AHD) epidemic model and the proposed CE-ABC algorithm. The plausible nominal values used in the integration of the dynamics of a virgin population for COVID-19 infections are presented in Table 1, which also shows numerical bounds (upper and lower) that are used to delineate the feasible domain limits in the CE method. The plausible values from Table 1 correspond to a COVID-19 outbreak in a virgin population to the disease, such as those observed worldwide in 2020. They were determined by information from the literature [3, 5, 19, 36, 39, 44, 57, 66, 71, 74, 78] or numerical experimentation.

Numerical experiments with these parameters are not focused on being very reliable reproductions of the COVID-19 outbreaks in 2020. They only aim to have the main characteristics of the epidemic dynamics so that they offer a good test for the methodology proposed in this paper.

The objective is to show that the CE-ABC framework can be used, together with a suitable epidemic model, in near real-time to predict the course of an epidemic outbreak of an emerging disease (such as COVID-19) in a time horizon compatible with the limits of predictability of the underlying dynamics.

### 4.1 Dynamic evolution of a fully susceptible population subjected to an initial infection

The first analysis presented here concerns the situation of a population virgin to COVID-19 infections, where the disease is introduced into the community by a single

individual externally exposed to the viral agent that causes the disease.

This is a hypothetical unrealistic case, as it does not consider any measures to mitigate or suppress the outbreak during its occurrence. However, its study may be essential to delineate a possible baseline behavior related to a potential epidemic of COVID-19, providing projections of a worst-case scenario and some intuition about the free evolution of the disease.

In this scenario, a constant value for  $\beta$  is considered, as well as an initial population  $N_0 = 5.5 \times 10^6$  (compatible with the city of Rio de Janeiro, Brazil), a single exposed individual  $E_0 = 1$ , and all other initial conditions are set to zero. The model parameters values are defined in the third column of Table 1.

The dynamic evolution of the SEIR(+AHD) model, for a temporal interval of 2 years, can be seen in Figure 5, which shows the corresponding time series in linear (top) and logarithmic (bottom) scales. In the bottom part, it is possible to better observe the trends of time series in which the maximum values are small compared to the initial size of the population.

Despite community transmission starting right in the first moments of the dynamics, due to the transmission structure of this type of model, an outbreak only takes on notable proportions after 200 days of disease circulation in the population. In other words, it may take more than six months after the start of transmission of the disease within this population for the outbreak to be noted by the major public.

However, after the outbreak became noticeable, a wave of contagion by COVID-19 quickly emerged, characterized by a rapid increase in exposed compartments, concomitant with a decrease at the same rate in the susceptible population. Most recover directly, while a small portion dies without medical care. The other part of those infected are hospitalized, most of them recover, and a small amount dies.

The peak of infections occurs around 350 days after the insertion of the first exposed case in the population, almost a year after the disease arrives in the community. There were about 700 thousand people with active disease (exposed, infectious and asymptomatic) in the community during the peak, almost 13% of the initial population. The susceptible corresponded to close to 20% of the people after two years, while the recovered account for almost 80% of the people.

The reader can better appreciate the evolution of the number of hospitalizations and new deaths per day in Figure 6 (top), as well as their respective cumulative values throughout the epidemic outbreak (bottom). The peaks of hospitalizations and deaths occur a few days after the peak of infections, involving more than

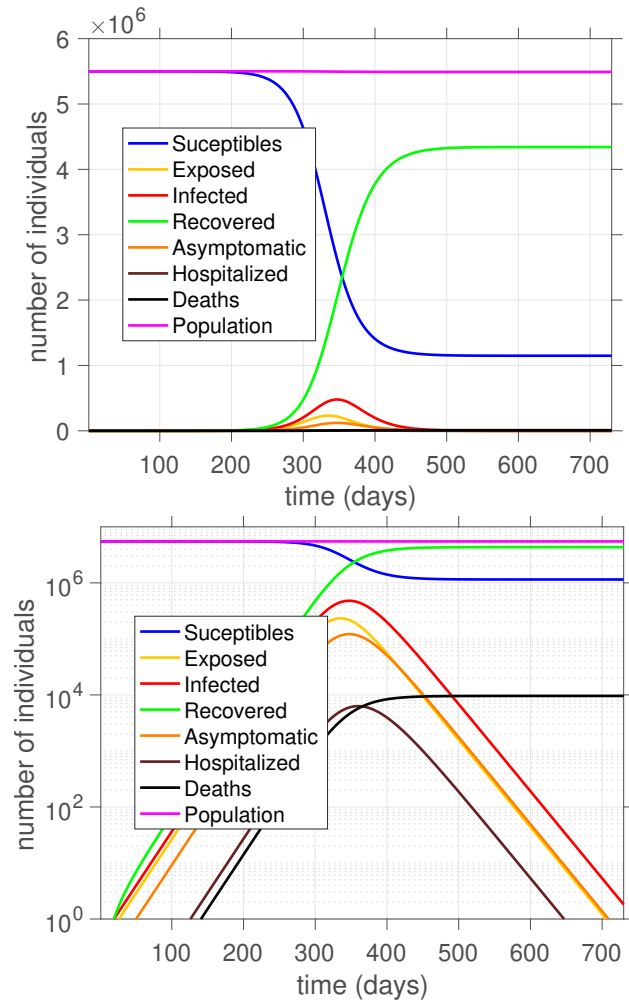


**Fig. 5** Dynamic response of the SEIR(+AHD) epidemic model in a scenario of a totally susceptible population, with a single individual exposed. Time series in linear scale are shown at the top and in logarithmic scale at the bottom, which allows displaying better the curves in which maximum values are small compared to the initial population value.

6000 people under medical care and around 100 deaths. At the end of the two-year window, almost 48,000 people were hospitalized at some point, and another 10,000 people died from complications inherent to the disease.

Throughout the outbreak, the variation in population size is slight compared to its initial size (10 thousand is a small number compared to 5.5 million, around 0.2%) but highly significant in demographic terms. This hypothetical outbreak is responsible for losing approximately 10 thousand lives in about 300 days. This value would correspond to something around 15% of all deaths that occurred in the city of Rio de Janeiro in 2019<sup>2</sup>. But note that, in this case, such an unusual amount of deaths is due to a single disease.

<sup>2</sup> Demographic data for the city of Rio de Janeiro can be available at <https://transparencia.registrocivil.org.br>.

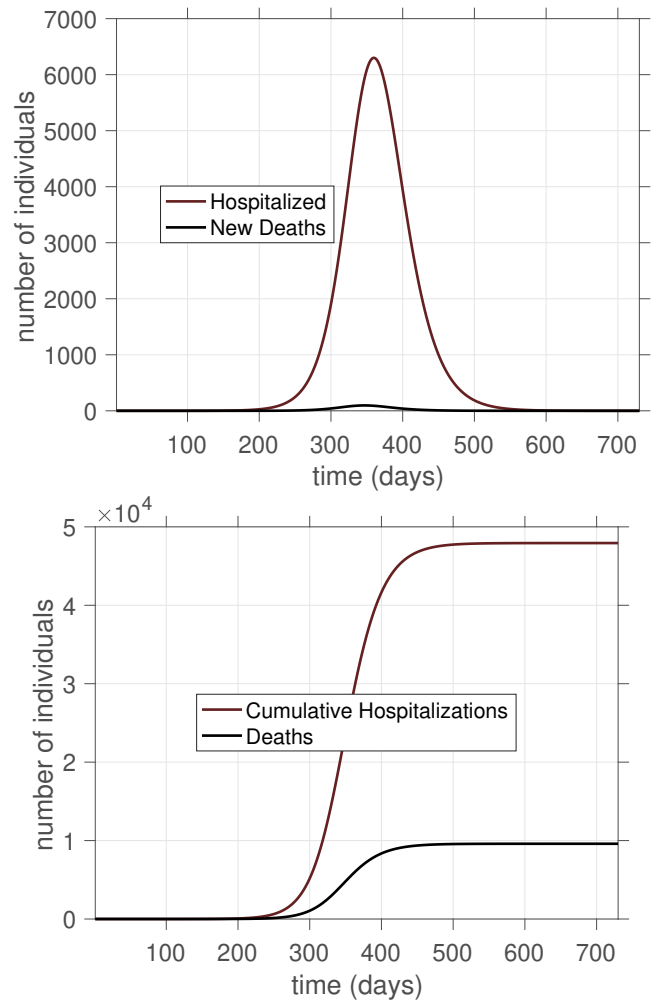


**Fig. 6** Dynamic response of the two QoIs for the SEIR(+AHD) epidemic model in a scenario of a totally susceptible population, with a single individual exposed. Time series for the number of hospitalized and new deaths are shown at the top, while the corresponding cumulative numbers can be seen at the bottom.

#### 4.2 Determination of a dynamically consistent initial state for the epidemic model calibration

Typically, in the process of calibrating a dynamic model with the aid of data, the bottleneck is identifying the initial conditions since, often, the initial state of the system of interest is partially (or even totally) unknown. This is the case when dealing with compartmentalized epidemic systems in the form of an SEIR model or its variants. Observations on the infected compartment are usually available (subject to delay and underreporting), but data from recovered rarely (and even when they are, they are often unreliable). However, for the practical impossibility of measuring them, the susceptible and exposed practically are never known directly. Other possible compartments can also be challenging to measure in practice [17,32].

In this scenario, the determination of initial conditions (or part of its components) is usually done via direct inference from the data [14,15,30,37] or by indirect means, with plausible assumptions or educated estimates about the actual values [6,41]. The latter approach is highly subject to epistemic errors, while the former may suffer from identifiability issues.

Note that by the existence and uniqueness theorem for ODEs [1,23,43,58,67], the dynamical system defined by (1) and a given initial condition has only one dynamic state for each instant of time. Once the value of one of the components is fixed (e.g. hospitalizations) for a particular moment, only one combination of values in the other compartments produces a dynamic state compatible with the fixed value. For this reason, it is practically impossible to infer a consistent initial condition from assumptions or ansatz to values (especially in an actual setting where surveillance data are imperfect representations of the dynamics of interest, and there are compartments for which data are not available).

To avoid the above difficulties, a three-step procedure to determine a suitable set of initial conditions that is compatible with the observed data is proposed:

1. Given a reference value for hospitalizations  $H_{ref}$ , the dynamics of a population virgin to the disease (such as presented in section 4.1) is used to determine the time instant for which  $H(t)$  is closest to  $H_{ref}$ . The corresponding dynamic state is recorded;
2. Analogously, given a reference value for deaths  $D_{ref}$ , the dynamic state corresponding to the shortest distance between  $D(t)$  and  $D_{ref}$  is obtained and recorded;
3. Finally, a dynamic state corresponding to a weighted average between the two states determined above is calculated and assumed to be a dynamically consistent initial condition.

When using the dynamics of a population totally susceptible to the disease to identify a dynamic state close to the reference values for  $H$  (or for  $D$ ), the procedure guarantees that this state is dynamically consistent, as it is a solution to the initial value problem associated with the epidemic model. Although, in general, such a state does not exactly satisfy the reference value, by the continuous dependence of the solutions on the initial conditions, one can guarantee that such a dynamic state is sufficiently close to the state associated with the exact value of the reference. By making a convex combination of initial conditions obtained this way, we still have a dynamic state close to all the reference values. In this way, the procedure described above can generate an initial condition that is dynamically consistent with the available data. The procedure is naturally

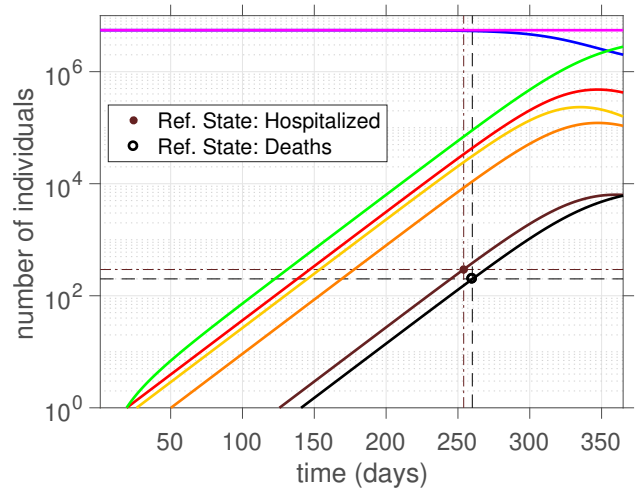


**Fig. 7** Determination of two distinct dynamic states of reference, the first obtained from hospitalization data and the second from death data. The figure also shows the time series of the SEIR(+AHD) model, on a semi-logarithmic scale, in a scenario of a totally susceptible population with a single exposed individual.

generalized if there are reference values for other compartments.

To illustrate of the methodology, the reader can observe Figure 7, which shows two distinct dynamic states obtained from the data on hospitalizations and deaths together with the time series on a semi-logarithmic scale, corresponding to the response of a virgin population to the disease with a single exposed individual. The convex combination of these two dynamic states, considering the same weights used in Eq.(11), is used as an initial condition in the numerical experiments presented in the following sections.

#### 4.3 Calibration and validation of the SEIR(+AHD) epidemic model and its descriptive capacity

In this section the proposed CE-ABC framework is used to calibrate and quantify the parametric uncertainties inherent to the SEIR(+AHD) dynamic model. To this end, the following hyperparameters are adopted in the CE-ABC algorithm: misfit function weight  $\omega = 0.75$  for hospitalizations (and thus,  $1 - \omega = 0.25$  for deaths); CE samples  $N_{ce} = 100$ ; CE elite sample set size  $N_{\mathcal{E}_\ell} = 10\%$  of  $N_{ce}$ ; CE absolute tolerance  $\text{atol} = 0.001$ ; CE relative tolerance  $\text{rtol} = 0.05$ ; CE mean value smoothing parameter  $a = 0.7$ ; CE variance dynamic smoothing parameters  $b = 0.8$  and  $q = 5$ ; CE maximum number of iterations  $\text{maxiter} = 150$ ; ABC samples  $N_{abc} = 2000$ ; ABC tolerance  $\text{tol} = 0.1$ . The bounds for the model parameters are adopted according to the values shown in Table 1.

**Table 2** Parameters identified for SEIR(+AHD) epidemic model via CE-ABC framework, and the respective standard deviation values.

|                      | Unit  | CE<br>Optimal | CE<br>std dev | ABC<br>Best | ABC<br>std dev |
|----------------------|-------|---------------|---------------|-------------|----------------|
| $\beta$ or $\beta_0$ | 1/day | 0.12          | 0.02          | 0.13        | 0.02           |
| $\alpha$             | 1/day | 0.20          | 0.07          | 0.27        | 0.06           |
| $f_E$                | —     | 0.81          | 0.03          | 0.84        | 0.03           |
| $\gamma$             | 1/day | 0.13          | 0.01          | 0.12        | 0.01           |
| $\rho$               | 1/day | 0.0006        | 0.0001        | 0.0005      | 0.0001         |
| $\delta$             | 1/day | 0.0021        | 0.0004        | 0.0015      | 0.0004         |
| $\kappa_A$           | —     | 0.0026        | 0.0008        | 0.0027      | 0.0008         |
| $\kappa_H$           | —     | 0.0563        | 0.0130        | 0.0575      | 0.0128         |
| $\epsilon_H$         | —     | 0.25          | 0.07          | 0.33        | 0.07           |
| $\beta_\infty$       | 1/day | 0.31          | 0.06          | 0.43        | 0.06           |
| $\eta$               | 1/day | 5.8           | 1.9           | 6.2         | 1.8            |
| $\tau_\beta$         | day   | 146           | 7             | 153         | 7              |

The data considered here for the training of the dynamic model include the records of hospitalizations and total deaths in the city of Rio de Janeiro between May 1 and 31, 2020. The statistical validation process of the calibrated model uses the data corresponding to the following month, between June 1 and 30, 2020. Data for April 2020 are ignored because they are unreliable since the city’s epidemiological surveillance system was still adapting to the new reality at the beginning of the pandemic.

The results regarding the calibration, quantification of uncertainties, and validation of the SEIR(+AHD) model with the aid of the CE-ABC algorithm can be seen in Table 2 and Figures 8 and 9.

Table 2 shows the values calculated by the CE-ABC algorithm for the parameters of the SEIR(+AHD) model, showing the estimates obtained by the CE optimizer in the third column; the respective standard deviation values in the fourth column; the best sample of the ABC simulation in the fifth column; and the standard deviation values of the posterior distributions obtained by ABC in the sixth column. The two sets of parameters identified present very close values, and the ABC result is a kind of refinement of the estimate obtained by the CE.

Regarding the posterior joint distribution of the model parameters, the reader finds this information in Figure 8, which presents the histograms and scatter plots for each of the model parameters (estimated with the samples accepted by the ABC simulation). Scatter plots give information about the correlation between the parameters. In this figure, the order of the parameters is the same as shown in Table 2.

In Figure 9 the reader can see the time series of hospitalizations (left) and total deaths (right) for the city of Rio de Janeiro in a time window that covers

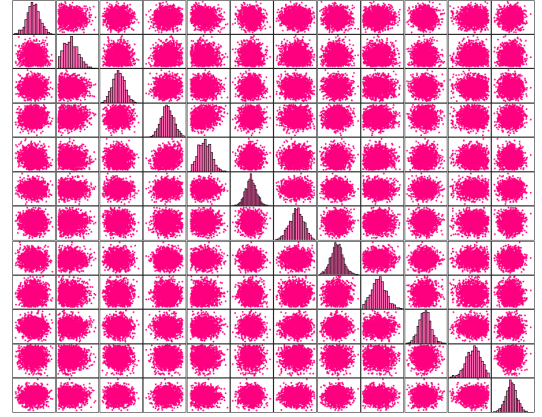


**Fig. 8** Histograms and scatter plots of the SEIR(+AHD) epidemic model, estimated with the samples accepted by the ABC simulations. The order of the parameters is the same as shown in Table 2.

the months of May and June 2020. Time trajectories, accepted by the ABC simulations (87% of the 2000 total)<sup>3</sup>, are displayed as thin solid lines in light gray; the trajectory that corresponds to the optimal set of parameters obtained by the CE optimizer is displayed as a dash-dotted line; the best sample trajectory obtained by the ABC simulation is indicated as a dashed line; while the median calculated with the samples accepted in the ABC simulation is indicated as a thick solid line. In addition, a 95% credibility envelope is displayed in the form of a filled region above the ABC samples. Training data are displayed as magenta circles, while validation data are shown as cyan asterisks.

The comparison between the CE-ABC time series and the training data shows that, in this scenario, the dynamic model can reproduce well the epidemic outbreak experienced by the city of Rio de Janeiro in May 2020. For both time series, the curve corresponding to the optimal set of parameters identified by the CE optimizer, the best scenario simulated by ABC, and the median calculated with the cases accepted in the ABC simulation provide good descriptions of the epidemic data trend. Furthermore, the training data fit is robust once it includes the 95% credibility interval obtained by ABC accepted samples, covering most of data fluctuations.

In terms of validation, by comparing the predictions (extrapolations) made by the dynamic model and future data (not used in the calibration), one can note that the dynamic model captures the trend of the out-

<sup>3</sup> This high acceptance rate, which may seem very high at first glance, is due to the informative prior obtained by CE.



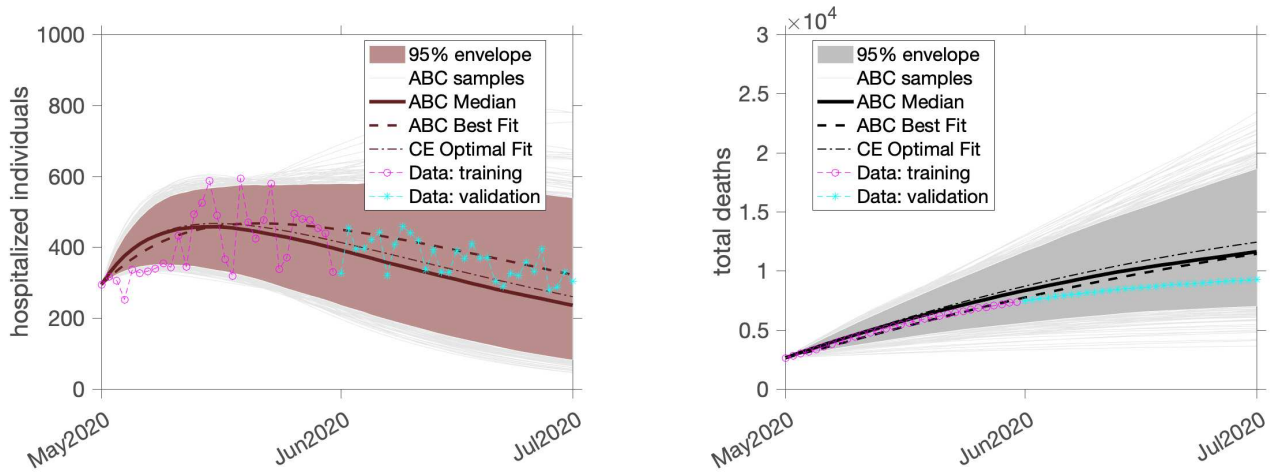


**Fig. 9** Time series generated by the CE-ABC algorithm for the number of hospitalized individuals (left) and total deaths (right) obtained with the SEIR(+AHD) model, which is calibrated with Rio de Janeiro epidemic data from May 2020 and validated for a temporal window covering the month of June 2020. Here the misfit function weight is  $\omega = 0.75$ , and ABC acceptance rate is 87%.

break. It takes over the data due to a 95% credibility band around the calculated evolution curves. Strictly speaking, the forecasts are reasonably accurate for the first seven days of extrapolation, starting to shift from the simulated curves from this point onwards. In what follows, hospitalizations are slightly underestimated by the ABC median by approximately 25%, while the median overestimates total deaths up to a limit of around 10%.

In light of the minimal horizon of predictability that epidemic systems present<sup>4</sup>, these predictions can be considered very good, as they provide accurate values in the short term (one week) and bring some reasonable information in the medium term (one month). Although 10-25% uncertainty in forecasting the number of hospital beds/expected deaths is not highly accurate for an immediate sizing of hospitals or funeral units, it is still informative in indicating to decision makers the correct order of magnitude for these outcomes. For instance, knowing a month in advance, in the course of an epidemic, that a few hundred (not thousands, or vice-versa) of hospital beds/burials will be required per day can be crucial information to prevent a hospital or cemetery from collapsing. Added to this is that the model can be recalibrated weekly (or daily), updating

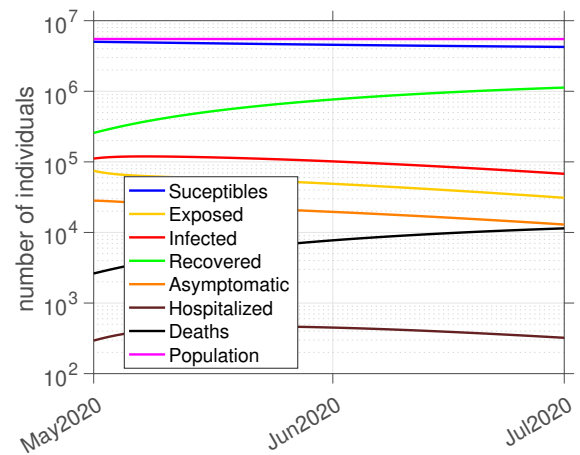


**Fig. 10** Dynamic response of the SEIR(+AHD) epidemic model, in a time window that includes the months of May and June 2020, considering the best estimate of the ABC simulation for the model parameters. Here the misfit function weight is  $\omega = 0.75$ .

the short/medium forecasts whenever new data become available.

It is also worth mentioning that, in addition to making predictions about the QoIs for which epidemic data are available, a well-calibrated mechanistic model can provide information on latent quantities (for which data are not available), such as the number of susceptible, exposed, asymptomatic, etc. In this sense, to illustrate this possibility, the reader is invited to observe Figure 10, which presents the evolution of the time series associated with eight dynamics state coordinates of the SEIR(+AHD) model in a time window that includes the months of May and June 2020, considering the best

<sup>4</sup> In an epidemic where people are aware of what is happening, there is a feedback between the rate of infection and people's social behavior. Being aware of the severity of the outbreak beforehand can help reduce its intensity or vice versa. The great difficulty in modeling such feedback is one of the factors (perhaps the main one) that limits the predictability horizon of epidemic models.

estimate of the ABC simulation for the model parameters.

From a qualitative point of view, this simulation allows the analyst to infer that, in this two-month interval, there is a slight but notable decrease in the number of susceptible people in the general population due to the increase in COVID-19 infections, followed by an increase in total recoveries. The number of symptomatic infected is always more significant than the number of exposed, greater than the asymptomatic infected. Quantitatively, it can be seen that these last three groups have sizes of the same order of magnitude, which is hundreds of times greater than the number of hospitalized patients. At the end of this two-month interval, the total number of accumulated deaths reaches a value comparable to the active infected.

Of course, the accuracy of such information largely depends on the extent to which the structure of the epidemic model provides a reliable representation of epidemic dynamics. If it is a good representation, the simulations should offer great insight; if it is a feeble representation, the simulations do not tell anything useful at the limit. In intermediate cases, where the model is more or less accurate, useful information can be obtained, but not all the information from the simulations is reliable. Separating what is helpful from what is not requires deep knowledge of some basic principles of epidemiology.

#### 4.4 Influence of CE-ABC hyperparameters on the description of the epidemic dynamical system

The CE-ABC framework combines two advanced stochastic simulation techniques, thus inheriting all the control parameters (a.k.a. hyperparameters) underlying the two methods. Consequently, the model calibration process and the propagation of parametric uncertainties depend, nonlinearly, on these hyperparameters. Thus, a study of how such quantities affect the modeling is desirable and recommendable. The present section of the manuscript seeks to shed light on this.

Initially, we investigated the effect of the misfit function weight parameter  $\omega$  on the results. Figure 11 presents the two QoIs calculated by the SEIR(+AHD) epidemic model, considering five different values for the weight:  $\omega \in \{0, 0.25, 0.5, 0.75, 1\}$ .

By visual inspection, it is possible to see that the best fits are obtained when  $\omega = 0.25$ ,  $\omega = 0.5$  or  $\omega = 0.75$ . The first and the last case favor one QoI, but without totally disregarding the effect of the other, while the intermediate case balances both. In this setting, deciding which QoI should be given more weight is

a matter of convenience. If the information on hospitalizations is more important, higher  $\omega$  values should be considered. The opposite is true if the primary interest is to follow the evolution of deaths.

The  $\omega = 0$  scenario considers a limiting case, where the misfit function defined by Eq.(11) considers only the total number of deaths. In contrast, considering only hospitalizations, the other extreme situation is counted when  $\omega = 1$ . These two limit cases have a terrible fit in the disregarded QoI, and should only be considered in situations in which only one of the QoI is of reliable.

Once the value of  $\omega$  is fixed, the results are also affected by the choices of  $\mathbf{x}_{min}$ ,  $\mathbf{x}_{max}$ ,  $N_{ce}$ ,  $N_{\mathcal{E}_\ell}$ ,  $N_{abc}$ , **atol**, **rtol**, **tol**, and **maxiter**.

The effect of varying the number ABC simulation samples  $N_{abc}$  can be seen in Figure 12, where results are presented for  $N_{abc} = 100$  (top) and  $N_{abc} = 1000$  (bottom). Note that the number of accepted samples is directly proportional to the total number of simulated samples. This variation directly impacts the estimation of the posterior distribution, with a consequence in the obtained median and credibility band. Of course, these estimates are also affected by the tolerance **tol**, which improves or worsens the results as it is decreased or increased. As it is an obvious effect, numerical experiments in this sense are not shown. A tolerance of the order of 10%, i.e., **tol** = 0.1, proved to be effective for the simulations in this paper.

The parameters **atol**, **rtol**, and **maxiter** have an influence on how much faster the CE optimizer will stop, with consequent gain/loss of accuracy, followed by an increase/decrease in the computational cost. The reader is invited to do numerical experiments with these parameters to see their effect in practice. In the preliminary numerical studies conducted by the authors, we observed that there are no great gains in obtaining an estimate of the optimal parameters with great precision. Relative tolerance values of the order of 5%, i.e., **rtol** = 0.05, provide a good compromise between accuracy and computational cost.

However, it is interesting to observe the effect of  $N_{ce}$  variation in practice, as shown in Figure 13, which considers different values for CE samples,  $N_{ce} = 50$  (top) and  $N_{ce} = 200$  (bottom). The number of CE samples influences the selection of the optimal set of parameters and the inference process performed by ABC, since the a priori distribution used by ABC is constructed with the help of statistics calculated by the CE. It is interesting to note that, unlike ABC, where a greater number of samples typically leads to a better inference result, this is not necessarily the case with CE optimization. In the example shown in Figure 13, the model calibrated with only 50 samples has better adherence to the data than



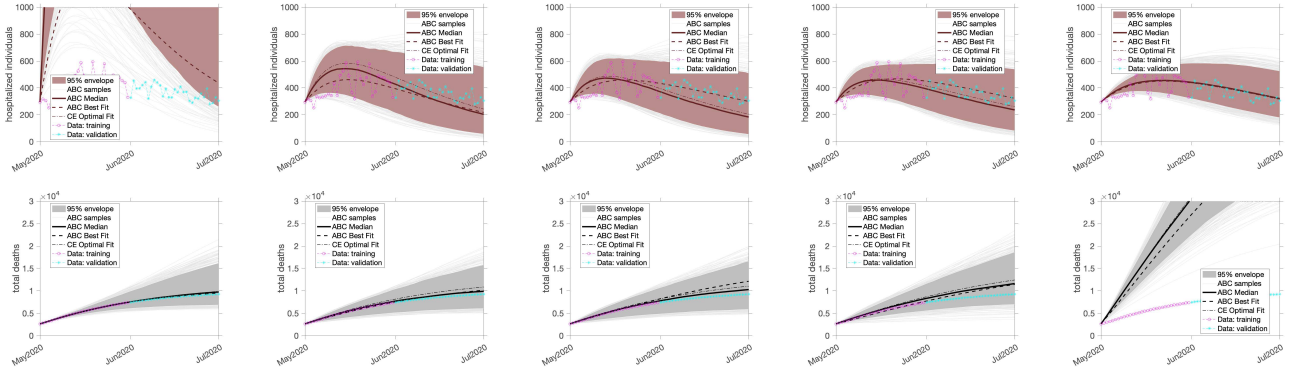


**Fig. 11** Quantities of interest calculated by the SEIR(+AHD) epidemic model with different values of the weight parameter:  $\omega = 0$  (first column);  $\omega = 0.25$  (second column);  $\omega = 0.5$  (third column);  $\omega = 0.75$  (fourth column);  $\omega = 1$  (fifth column).

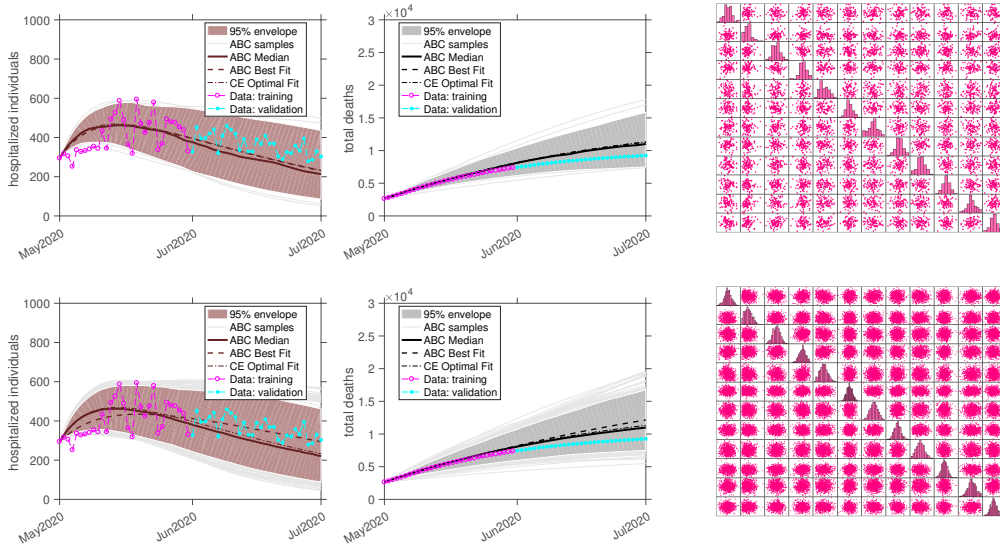


**Fig. 12** Effect of varying the number ABC simulation samples on the QoIs calculations and posterior inference. At the top  $N_{abc} = 100$ , while at the bottom  $N_{abc} = 1000$ . Here the misfit function weight is  $\omega = 0.75$  and  $N_{ce} = 100$ .

the counterpart that uses  $N_{ce} = 200$ . A variation in the size of the elite set  $N_{\mathcal{E}_\ell}$  can positively or negatively impact accuracy, depending on the case. Prior numerical experiments help identifying which case of the problem of interest.

As it is a stochastic algorithm, obviously the results depend on the value of the statistical seed used. Figure 14 shows two simulations with the same hyperparameters, but with slightly different inference results.

Finally, but not least, it is worth mentioning that the results are strongly influenced by choice of bounds  $\mathbf{x}_{min}$  and  $\mathbf{x}_{max}$ . Indeed, in the authors' experience, these are the parameters that have the most significant impact on the quality of results (together with the epidemic surveillance data). A bad choice for the parameter bounds can lead to unreliable models for the actual behavior of the outbreak. Good choices for these parameters demand detailed knowledge about the biological

aspects of the problem. Numerical experimentation can also be of great help in finding plausible values.

#### 4.5 Predictability limit for the epidemic dynamics using the CE-ABC and the SEIR(+AHD) model

To conclude the presentation and discussion of the results, this section presents a study to delineate the predictability limit of the SEIR(+AHD) model as a tool to predict the dynamics of COVID-19 in the city of Rio de Janeiro in the year 2020.

To this end, Figures 15 and 16 show the evolution of the two QoIs, for various training data sets, extrapolating forecasts over a 30-day horizon. Training data are incremented every seven days, including information from the last seven days, starting with the period

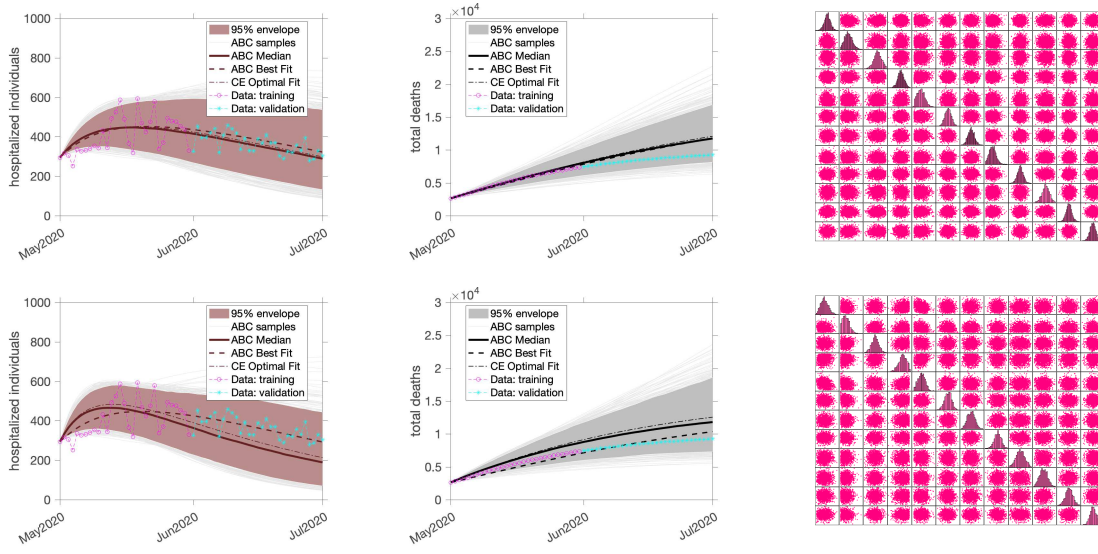


**Fig. 13** Effect of varying the number CE samples on the QoIs calculations and posterior inference. At the top  $N_{ce} = 50$ , while at the bottom  $N_{ce} = 200$ . Here the misfit function weight is  $\omega = 0.75$  and  $N_{abc} = 2000$ .

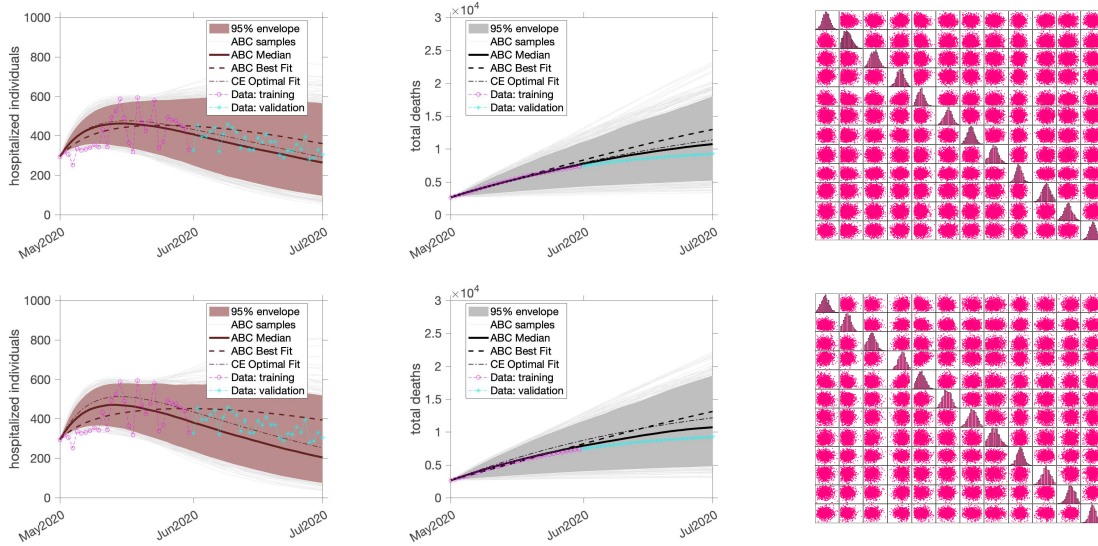


**Fig. 14** Effect of the statistical seed on the QoIs calculations and posterior inference. Here the misfit function weight is  $\omega = 0.75$ ,  $N_{abc} = 2000$  and  $N_{ce} = 200$ .

between May 1 and 7, 2020, and ending with May 1 and July 9, 2020.

For the first three calibrations (calibrations between the first and third week), the model presents a modest descriptive capacity of the data, with the trend of the short and mid-term forecasts being quite discrepant to that observed in the following weeks. However, the respective credibility intervals encompass the observations.

As the weeks go by, with more (and better quality) data feeding into the model (calibrations between the fourth and seventh week), the description of the

training data improves substantially, as does the predictive ability. In such cases, within a week, the model's median predicts the numbers of hospitalizations and deaths with reasonable accuracy for epidemic estimates. However, it starts to lose accuracy from the second week of extrapolation gradually, although it continues to follow, more or less, the trend of the data for 30 days (and covers them via the credibility band).

The descriptive capacity remains impeccable for the last three weeks of model calibration (weeks eight to ten), with good short-term (one week) prediction. However, it is possible to notice a significant divergence be-

tween predictions and observations after seven days of extrapolation. Such a loss of predictability is not directly related to the quantity or quality of the calibration data but rather to a structural change in the dynamic behavior of the outbreak. In July 2020, the second wave of contagion began in the city of Rio de Janeiro [18], drastically changing the trend of evolution of QoIs. As the infection rate  $\beta(t)$  was modeled to only contemplate a single change in the infection plateau, the present model cannot accurately describe the new wave of infections. One possibility to make the model regain its predictive capacity would be the inclusion of a new infection plateau in Eq.(2), as done in [66]. In general, this strategy can be adopted to address not just one but several waves of infection. Due to space limitations, the authors did not include results in this sense in the manuscript, but it would be interesting to test this strategy in future work.

The above results show that the model's descriptive capacity and predictability limit are strongly influenced by the amount and quality of data used in the calibration process.

In general, the more data, the greater the predictability horizon of the model. It presents an excellent or good capacity to extrapolate within a horizon of one or two weeks, with some capacity to predict the trend up to thirty days (depending on the outbreak's dynamic behavior). The quality of the outbreak's data also matters, as it is clear from the first three numerical experiments. In these cases, hospitalization data do not show the typical fluctuation of this time series (probably due to underreporting, since at the beginning of May 2020, the surveillance system in Rio de Janeiro was still adapting to the pandemic), which affects the model's fitting.

Insufficient or poor quality data can compromise the model's fit, generating unrealistic predictions. However, structural changes in the dynamic behavior of the epidemic (e.g., the emergence of a new wave of contagion) have an even more pronounced effect in compromising the predictive capacity of the model. In the periods preceding such changes, even quality data cannot guarantee that the model will extrapolate the data well in the mid (or even in the short) term.

## 5 Concluding remarks

### 5.1 Contributions

This paper proposes a new calibration procedure that combines cross-entropy optimization (CE) with approximate Bayesian computation (ABC). In the first step, CE is used to obtain an initial and informative estimation of the model parameters. Then, central tendency

and dispersion pieces of information obtained from CE are used to construct a informative prior distribution for an inference process that uses ABC to refine the model calibration and propagate the underlying uncertainties via rejection-sampling Monte Carlo simulation.

This combination of well-established algorithms gives rise to a framework for uncertainty quantification with several good features. CE and ABC are intuitive and straightforward algorithms, their combination gives rise to a simplistic framework, with few control parameters of clear interpretation, where no gradient computation is required, capable of performing robust inferences with good computational efficiency. In the update step with ABC, the initial knowledge about the model parameters obtained by CE optimization is incorporated into the prior distribution, updated with the aid of the available data to produce an informative posterior distribution. Also, there is no need to assume an additive Gaussian model. The uncertainty propagation is performed when the parameters are identified, generating considerable computational savings. The major limitation of the methodology has to do with its sampling nature, so many simulations might be needed to achieve convergence. This characteristic is not a problem for applications using epidemic models based on differential equations, where each deterministic simulation has a low computational cost. But for other domains, where models may take hours/days to run a single instance, the CE-ABC framework may not be competitive.

The proposed methodology was tested on an epidemic model with an SEIR-type structure that also considers asymptomatic individuals, hospitalizations, deaths, and time-dependent transmission rate. Actual data from COVID-19 outbreaks in Rio de Janeiro city were employed in the model calibration process. The results were consistent, and the methodology seems promising. They show that it is possible to perform good calibrations of the epidemic model with the CE-ABC formalism in scenarios that require a descriptive model (to explain past outbreaks) and those where the objective is to obtain a predictive model (to infer future behavior of epidemics). In scenarios where the epidemic model structure is a good abstraction of the contagion dynamics, a horizon of good quantitative predictability of up to two weeks can be achieved using CE-ABC for model calibration and uncertainty quantification, with a good capacity for qualitative description of the data trend for up to one month.

### 5.2 Future directions

There are some possibilities to continue this research. One can apply the proposed methodology to other dy-

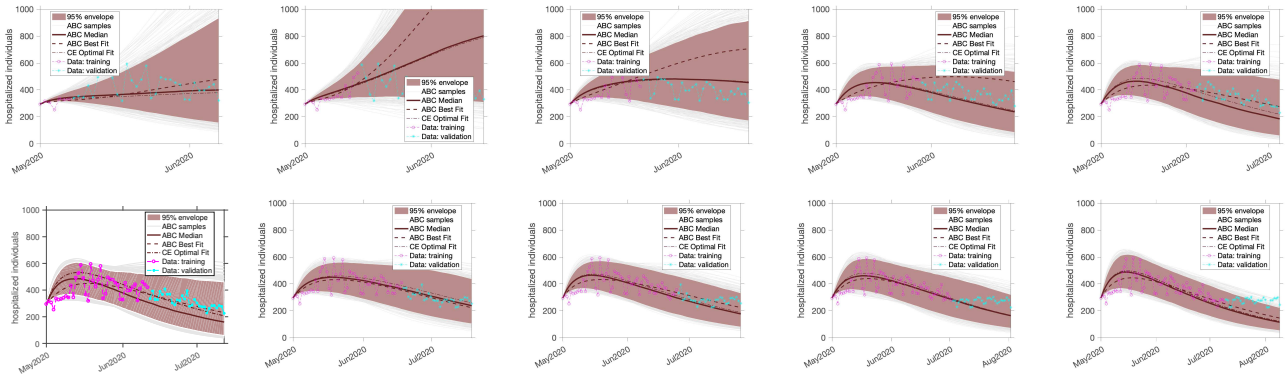


**Fig. 15** Evolution of the hospitalizations time series, calibrated with different datasets of Rio de Janeiro epidemic, extrapolating forecasts over a 30-day horizon. Training data are incremented every seven days, including information from the last seven days, starting with the period between May 1 and 7, 2020, and ending with May 1 and July 9, 2020.

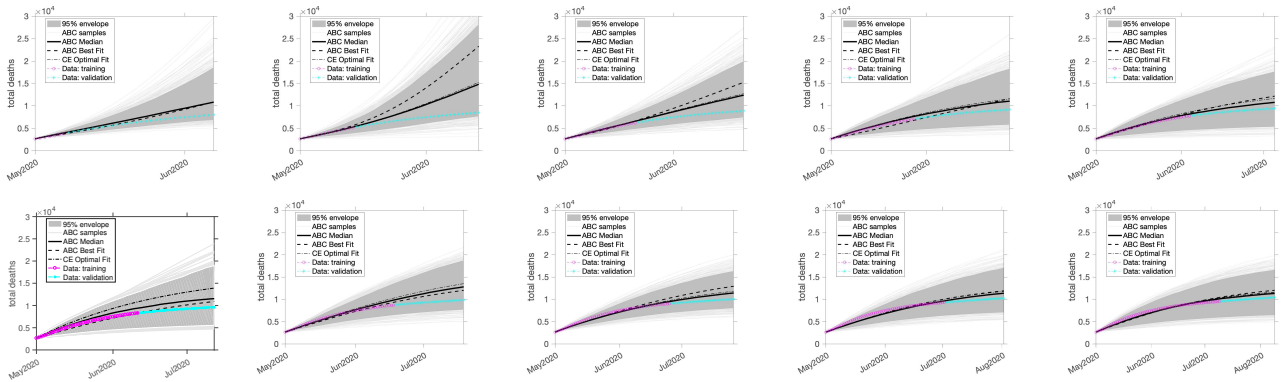


**Fig. 16** Evolution of the total deaths time series, calibrated with different datasets of Rio de Janeiro epidemic, extrapolating forecasts over a 30-day horizon. Training data are incremented every seven days, including information from the last seven days, starting with the period between May 1 and 7, 2020, and ending with May 1 and July 9, 2020.

namical systems, including other COVID-19 models with different data, or the possibility of contemplating multiple waves of infection. Another branch that can be explored is related to model (epistemic) uncertainties. For instance, it can be very appealing to combine our CE-ABC framework with methodologies that compensate for deficiencies in the structure of the mathematical model. For instance, the random matrix-based non-parametric probabilistic approach by C. Soize [55]; the universal differential equations (UDE) for scientific machine learning by Rackauckas et al. [45]; or one of the physics-informed neural networks approached for epidemic modeling available on the literature [28,47,51,75]. It would also be exciting and natural to insert the CE-ABC algorithm proposed here as a calibration a UQ module in the integrated framework for data-driven epidemic models developed by Zhang et al. [77].

### 5.3 Disclaimer

A model is always wrong, but some of them are useful. This idea has a more pronounced meaning in computational epidemiology than in physics, as the first principles of epidemic dynamics are unknown. Although a mechanistic model such as the SEIR(+AHD) used here is a (typically very rough) approximation of epidemic dynamics, it allows exploring qualitative scenarios (short, medium, and long term) that can provide great insight into the evolution of the outbreak. Thus, being an extremely valuable tool for epidemiologists [24]. Undoubtedly, such an approach is much more rational and conservative than being guided by the (well-intentioned or not) opinion of curious people with no training in the area or the general public (layman by definition).

However, a final observation is necessary before one uses an epidemic model to guide decision-making during a real-time outbreak. It concerns the interpretation of results. As epidemiology is a highly interdisciplinary area, it is practically impossible for a single professional

to hold all the necessary skills to assess the results of an epidemic simulation unequivocally and, above all, understand the consequences of intervention measures that can be taken. Scientific, ethical, and humanistic aspects are equally important in this context and need to be discussed by an interdisciplinary panel of professionals. In this sense, the authors of this paper strongly recommend that simulations of this nature, especially made with our model and framework, be evaluated and used with great caution when making decisions, preferably being scrutinized by a team of experts.

## Dedication

The authors dedicate this work to the memory of all the victims of the COVID-19 worldwide tragedy. In particular, the first author dedicates the paper to his friends Natasha Zadorosny and Victor Costa Silva, who left in their prime.

## Funding

The first author received financial support from the Carlos Chagas Filho Research Foundation of Rio de Janeiro State (FAPERJ) under the following grants: 210.167/2019, 211.037/2019, and 201.294/2021. The second author would like to acknowledge the Engineering and Physical Sciences Research Council (EPSRC) via grant number EP/R006768/1. The last author would like to acknowledge the financial support from the Brazilian agencies *Coordenação de Aperfeiçoamento de Pessoal de Nível Superior* (CAPES) under the grants Finance Code 001, PROEX 803/2018, and CAPES-PRINT 88887.569759/2020-00, and FAPERJ under the grant E-26/201.183/2022.

## Code availability

To facilitate the reproduction of this paper's results the code used in the simulations is available on GitHub:

<https://github.com/americocunhajr/CE-ABC>

## Declarations

## Conflict of Interest

The authors declares that they have no conflict of interest.

## References

1. Arnold, V.I.: Ordinary Differential Equations, 2nd edn. Springer (1992)
2. Brauer, F.: Mathematical epidemiology: Past, present, and future. *Infectious Disease Modelling* **2**(2), 113–127 (2017). DOI 10.1016/j.idm.2017.02.001
3. Byambasuren, O., Cardona, M., Bell, K., Clark, J., McLaws, M.L., Glasziou, P.: Estimating the extent of asymptomatic COVID-19 and its potential for community transmission: Systematic review and meta-analysis. *Official Journal of the Association of Medical Microbiology and Infectious Disease Canada* **5**(4), 223–234 (2020). DOI 10.3138/jammi-2020-0030
4. Cai, M., Karniadakis, G.E., Li, C.: Fractional SEIR model and data-driven predictions of COVID-19 dynamics of Omicron variant (2022). DOI 10.48550/arxiv.2205.11379
5. Cheng, C., et al.: The incubation period of COVID-19: a global meta-analysis of 53 studies and a Chinese observation study of 11 545 patients. *Infectious Diseases of Poverty* **10**(1), 119 (2021). DOI 10.1186/s40249-021-00901-9
6. Costa, G.S., Cota, W., Ferreira, S.C.: Outbreak diversity in epidemic waves propagating through distinct geographical scales. *Physical Review Research* **2**, 043306 (2020). DOI 10.1103/PhysRevResearch.2.043306
7. Cotta, R.M., Naveira-Cotta, C.P., Magal, P.: Mathematical parameters of the COVID-19 epidemic in Brazil and evaluation of the impact of different public health measures. *Biology* **9**(8) (2020). DOI 10.3390/biology9080220
8. Cunha Jr, A.: Modeling and Quantification of Physical Systems Uncertainties in a Probabilistic Framework. In: S. Ekwaro-Osire, A.C. Goncalves, F.M. Alemayehu (eds.) *Probabilistic Prognostics and Health Management of Energy Systems*, pp. 127–156. Springer International Publishing, New York (2017). DOI 10.1007/978-3-319-55852-3\_8
9. Cunha Jr, A.: Enhancing the performance of a bi-stable energy harvesting device via the cross-entropy method. *Nonlinear Dynamics* **103**, 137–155 (2021). DOI 10.1007/s11071-020-06109-0
10. Cunha Jr, A., Nasser, R., Sampaio, R., Lopes, H., Breitman, K.: Uncertainty quantification through Monte Carlo method in a cloud computing setting. *Computer Physics Communications* **185**, 1355–1363 (2014). DOI 10.1016/j.cpc.2014.01.006
11. Dantas, E.: A cross-entropy strategy for parameters identification problems. Monograph, Universidade do Estado do Rio de Janeiro (2019). <https://dx.doi.org/10.13140/RG.2.2.18045.51688>
12. Dantas, E., Cunha Jr, A., Silva, T.A.N.: A numerical procedure based on cross-entropy method for stiffness identification. In: *5th International Conference on Structural Engineering Dynamics (ICEDyn 2019)*. Viana do Castelo, Portugal (2019)
13. Dantas, E., Cunha Jr, A., Soeiro, F.J.C.P., Cayres, B.C., Weber, H.I.: An inverse problem via cross-entropy method for calibration of a drill string torsional dynamic model. In: *25th ABCM International Congress of Mechanical Engineering (COBEM 2019)*. Uberlândia, Brazil (2019)
14. Dantas, E., Tosin, M., Cunha Jr, A.: Calibration of a SEIR-SEI epidemic model to describe Zika virus outbreak in Brazil. *Applied Mathematics and Computation* **338**, 249–259 (2018). DOI 10.1016/j.amc.2018.06.024



15. Dantas, E., Tosin, M., Cunha Jr, A.: An uncertainty quantification framework for a Zika virus epidemic model. *Journal of Computational Interdisciplinary Sciences* **10**, 91 (2019)
16. De Boer, P.T., Kroese, D.P., Mannor, S., Rubinstein, R.Y.: A tutorial on the cross-entropy method. *Annals of Operations Research* **134**, 19–67 (2005). DOI 10.1007/s10479-005-5724-z
17. Gamerman, D., Prates, M.O., Paiva, T., Mayrink (Editors), V.D.: Building a Platform for Data-Driven Pandemic Prediction From Data Modelling to Visualisation - The CovidLP Project. Chapman and Hall/CRC (2022)
18. Gianfelice, P.R.L., Oyarzabal, R.S., Cunha, A., Grzybowski, J.M.V., Batista, F.C., Macau, E.E.N.: The starting dates of COVID-19 multiple waves. *Chaos: An Interdisciplinary Journal of Nonlinear Science* **32**(3), 031101 (2022). DOI 10.1063/5.0079904
19. Grasselli, G., Zangrillo, A., Zanella, A., Antonelli, M., Cabrini, L., Castelli, A., Cereda, D., Coluccello, A., Foti, G., Fumagalli, R., Iotti, G., Latronico, N., Lorini, L., Merler, S., Natalini, G., Piatti, A., Ranieri, M.V., Scandroglio, A.M., Storti, E., Cecconi, M., Pesenti, A., Network, C.L.I.: Baseline Characteristics and Outcomes of 1591 Patients Infected With SARS-CoV-2 Admitted to ICUs of the Lombardy Region, Italy. *Journal of the American Medical Association* **323**(16), 1574–1581 (2020). DOI 10.1001/jama.2020.5394
20. He, S., Peng, Y., Sun, K.: SEIR modeling of the COVID-19 and its dynamics. *Nonlinear Dynamics* **101**(3), 1667–1680 (2021). DOI 10.1007/s11071-020-05743-y
21. Hethcote, H.W.: The mathematics of infectious diseases. *SIAM Review* **42**(4), 599–653 (2000). DOI 10.1137/S0036144500371907
22. Hindmarsh, A.C., Brown, P., Grant, K., Lee, S., Serban, R., Shumaker, D.E., Woodward, C.S.: SUNDIALS: Suite of Nonlinear and Differential/Algebraic Equation Solvers. *ACM Transactions on Mathematical Software* **31**(3), 363–396 (2005). DOI 10.1145/1089014.1089020
23. Hirsch, M.W., Smale, S., Devaney, R.L.: *Differential Equations, Dynamical Systems, and an Introduction to Chaos*, 3rd edn. Academic Press (2012)
24. Holmdahl, I., Buckee, C.: Wrong but Useful — What Covid-19 Epidemiologic Models Can and Cannot Tell Us. *New England Journal of Medicine* **383**(4), 303–305 (2020). DOI 10.1056/NEJMp2016822
25. Jaynes, E.T.: *Probability Theory: the logic of science*. Cambridge University Press (2003)
26. Jha, P., Cao, L., Oden, J.: Bayesian-based predictions of COVID-19 evolution in Texas using multispecies mixture-theoretic continuum models. *Computational Mechanics* **66**(5), 1055–1068 (2020). DOI 10.1007/s00466-020-01889-z
27. Kaipio, J., Somersalo, E.: *Statistical and Computational Inverse Problems*. Springer (2004)
28. Kharazmi, E., Cai, M., Zheng, X., Zhang, Z., Lin, G., Karniadakis, G.E.: Identifiability and predictability of integer- and fractional-order epidemiological models using physics-informed neural networks. *Nature Computational Science* **1**(11), 744–753 (2021). DOI 10.1038/s43588-021-00158-0
29. Kroese, D.P., Taimre, T., Botev, Z.I.: *Handbook of Monte Carlo Methods*. Wiley (2011)
30. Kucharski, A.J., Funk, S., Eggo, R.M., Mallet, H.P., Edmunds, W.J., Nilles, E.J.: Transmission dynamics of Zika virus in island populations: a modelling analysis of the 2013–14 French Polynesia outbreak. *PLoS Neglected Tropical Diseases* **10**(5) (2016). DOI 10.1371/journal.pntd.0004726
31. Kucharski, A.J., Russell, T.W., Diamond, C., Liu, Y., J., E., Funk, S., Eggo, R.M.: Early dynamics of transmission and control of COVID-19: a mathematical modelling study. *The Lancet Infectious Diseases* **20**(5), 553–558 (2020). DOI 10.1016/S1473-3099(20)30144-4
32. Kuhl, E.: *Computational Epidemiology: Data-Driven Modeling of COVID-19*. Springer (2021)
33. Lobato, F.S., Libotte, G.B., Platt, G.M.: Mathematical modelling of the second wave of COVID-19 infections using deterministic and stochastic SIRD models. *Nonlinear Dynamics* **106**, 1359–1373 (2021). DOI 10.1007/s11071-021-06680-0
34. Lyra, W., do Nascimento, J.D., Belkhiria, J., de Almeida L., Chrispim, P.P.M., de Andrade, I.: COVID-19 pandemics modeling with modified determinist SEIR, social distancing, and age stratification. the effect of vertical confinement and release in Brazil. *PLoS ONE* **15**(9), e0237627 (2020). DOI 10.1371/journal.pone.0237627
35. Martcheva, M.: *An Introduction to Mathematical Epidemiology*. Springer, New York (2015)
36. MIDAS Network: MIDAS 2019 Novel Coronavirus Repository. <https://github.com/midas-network/COVID-19> (2020)
37. Morrison, R.E., Cunha Jr, A.: Embedded model discrepancy: A case study of Zika modeling. *Chaos: An Interdisciplinary Journal of Nonlinear Science* **30**, 051103 (2020). DOI 10.1063/5.0005204
38. Müller, J., Kuttler, C.: *Methods and Models in Mathematical Biology: Deterministic and Stochastic Approaches*. Springer, New York (2015)
39. Nogrady, B.: What the data say about asymptomatic COVID infections. *Nature* **587**, 534–535 (2020). DOI 10.1038/d41586-020-03141-3
40. Oliveira, J.F., Jorge, D.C.P., Veiga, R.V., Rodrigues, M.S., Torquato, M.F., da Silva, N.B., Fiaccone, R.L., Cardim, L.L., Pereira, F.A.C., de Castro, C.P., Paiva, A.S.S., Amad, A.A.S., Lima, E.A.B.F., Souza, D.S., Pinho, S.T.R., Ramos, P.I.P., Andrade, R.F.S.: Mathematical modeling of COVID-19 in 14.8 million individuals in Bahia, Brazil. *Nature Communications* **12**, 333 (2021). DOI 10.1038/s41467-020-19798-3
41. Pacheco, P.M.C.L., Savi, M.A., Savi, P.V.: COVID-19 dynamics considering the influence of hospital infrastructure: an investigation into Brazilian scenarios. *Nonlinear Dynamics* **106** (2021). DOI 10.1007/s11071-021-06323-4
42. Pavlack, B., Grave, M., Dantas, E., Basilio, J., de la Roca, L., Norenberg, J.a., Tosin, M., Chaves, L., Matos, D., Issa, M., Luo, R., Guyt, A., Soares, L., Burgos, R., Lovisol, L., Cunha, A.: EPIDEMIC - Epidemiology Educational Code. *Journal of Open Source Education* **5**, 149 (2022). DOI 10.21105/jose.00149
43. Perko, L.: *Differential Equations and Dynamical Systems*, 3rd edn. Springer (2006)
44. Prefeitura do Rio de Janeiro: Painel Rio COVID-19. <http://coronavirus.rio/painel> (2022)
45. Rackauckas, C., Ma, Y., Martensen, J., Warner, C., K, Z., Supekar, R., Skinner, D., Ramadhan, A., Edelman, A.: Universal differential equations for scientific machine learning. arxiv p. 2001.04385 (2020). DOI 10.48550/arXiv.2001.04385
46. Rahman, S., Rahman, M.M., Miah, M., Begum, M.N., Sarmin, M., Mahfuz, M., Hossain, M.E., Rahman, M.Z., Chisti, M.J., Ahmed, T., Arifeen, S.E., Rahman, M.: COVID-19 reinfections among naturally infected and

- vaccinated individuals. *Scientific Reports* **12**, 1438 (2022). DOI 10.1038/s41598-022-05325-5
47. Raissi, M., Ramezani, N., Seshaiyer, P.: On parameter estimation approaches for predicting disease transmission through optimization, deep learning and statistical inference methods. *Letters in Biomathematics* **6**(2), 1–26 (2019). DOI 10.1080/23737867.2019.1676172
48. Rubinstein, R.Y.: The cross-entropy method for combinatorial and continuous optimization. *Methodology and Computing in Applied Probability* **2**, 127–190 (1999). DOI <https://doi.org/10.1023/A:1010091220143>
49. Rubinstein, R.Y.: *Simulation and the Monte Carlo Method*, 3rd edn. Wiley (2016)
50. Rubinstein, R.Y., Kroese, D.P.: *The Cross-Entropy Method: A Unified Approach to Combinatorial Optimization, Monte-Carlo Simulation and Machine Learning*. Information Science and Statistics. Springer-Verlag (2004)
51. Shaier, S., Raissi, M., Seshaiyer, P.: Data-driven approaches for predicting spread of infectious diseases through DINNs: Disease Informed Neural Networks (2021). DOI 10.48550/arxiv.2110.05445
52. Shampine, L.F., Reichelt, M.W.: The MATLAB ODE Suite **18**(1), 1–22 (1997). DOI 10.1137/S1064827594276424
53. Sivia, D.S.: *Data analysis – a Bayesian tutorial*. Oxford Science (2006)
54. Smith, R.C.: *Uncertainty Quantification: Theory, Implementation and Applications*. SIAM (2014)
55. Soize, C.: A nonparametric model of random uncertainties for reduced matrix models in structural dynamics. *Probabilistic Engineering Mechanics* **15**(3), 277–294 (2010). DOI 10.1016/S0266-8920(99)00028-4
56. Soize, C.: *Uncertainty Quantification: An Accelerated Course with Advanced Applications in Computational Engineering*. Springer (2017)
57. Statista: Coronavirus (COVID-19) death rate in countries with confirmed deaths and over 1,000 reported cases as of november 2, 2021, by country. <https://www.statista.com/statistics/1105914/coronavirus-death-rates-worldwide/> (2021)
58. Strogatz, S.H.: *Nonlinear Dynamics and Chaos: With Applications To Physics, Biology, Chemistry, And Engineering*, 2nd edn. Westview Press (2014)
59. Sunnåker, M., Busetto, A.G., Numminen, E., Corander, J., Foll, M., Dessimoz, C.: Approximate Bayesian Computation. *PLOS Computational Biology* **9**(1), 1–10 (2013). DOI 10.1371/journal.pcbi.1002803
60. Taghizadeh, L., Karimi, A., Heitzinger, C.: Uncertainty quantification in epidemiological models for the COVID-19 pandemic. *Computers in Biology and Medicine* **125**, 104011 (2020). DOI 10.1016/j.compbiomed.2020.104011
61. Tarantola, A.: *Inverse Problem Theory and Methods for Model Parameter Estimation*. SIAM (2005)
62. Tenorio, L.: *An Introduction to Data Analysis and Uncertainty Quantification for Inverse Problems*. SIAM (2017)
63. Tolles, J., Luong, T.: Modeling Epidemics With Compartmental Models. *Journal of the American Medical Association* **323**(24), 2515–2516 (2020). DOI 10.1001/jama.2020.8420
64. Toni, T., Welch, D., Strelkowa, N., Ipsen, A., Stumpf, M.P.H.: Approximate Bayesian computation scheme for parameter inference and model selection in dynamical systems. *Journal of the Royal Society Interface* **6**(31), 187–202 (2009). DOI 10.1098/rsif.2008.0172
65. Tosin, M.: Modeling and uncertainty quantification in the nonlinear dynamics of epidemiological phenomena: Application to Zika virus and COVID-19 outbreaks. Master’s thesis, Universidade do Estado do Rio de Janeiro, Rio de Janeiro (2021)
66. Vasconcelos, G.L., Brum, A.A., Almeida, F.A.G., Macêdo, A.M.S., Duarte-Filho, G.C., Ospina, R.: Standard and anomalous waves of COVID-19: A multiple-wave growth model for epidemics. *Brazilian Journal of Physics* **51**, 1867–1883 (2021). DOI 10.1007/s13538-021-00996-3
67. Verhulst, F.: *Nonlinear Differential Equations and Dynamical Systems*, 2nd edn. Springer (2012)
68. Vyasrayani, C.P., Chatterjee, A.: New approximations, and policy implications, from a delayed dynamic model of a fast pandemic. *Physica D: Nonlinear Phenomena* **414**, 132701 (2021). DOI 10.1016/j.physd.2020.132701
69. Vynnycky, E., White, R.: *An Introduction to Infectious Disease Modelling*. Oxford University Press (2010)
70. Wang, B.: Parameter estimation for ODEs using a cross-entropy approach. Master’s thesis, University of Toronto, Toronto (2012)
71. Wang, D., et al.: Clinical characteristics of 138 hospitalized patients with 2019 novel coronavirus-infected pneumonia in Wuhan, China. *Journal of the American Medical Association* **323**(11), 1061–1069 (2021). DOI 10.1001/jama.2020.1585
72. Weitz, J.S., Park, S.W., Eksin, C., Dushoff, J.: Awareness-driven behavior changes can shift the shape of epidemics away from peaks and toward plateaus, shoulders, and oscillations. *Proceedings of the National Academy of Sciences* **117**(51), 32764–32771 (2020). DOI 10.1073/pnas.2009911117
73. WHO: Coronavirus disease 2019 (COVID-19). Situation report 24. Geneva: World Health Organization (2020)
74. Wu, P., Hao, X., Lau, E.H.Y., Wong, J.Y., Leung, K.S.M., Wu, J.T., Cowling, B.J., Leung, G.M.: Real-time tentative assessment of the epidemiological characteristics of novel coronavirus infections in wuhan, china, as at 22 january 2020. *Eurosurveillance* **25**(3), (2020). DOI 10.2807/1560-7917.es.2020.25.3.2000044
75. Yazdani, A., Lu, L., Raissi, M., Karniadakis, G.E.: Systems biology informed deep learning for inferring parameters and hidden dynamics. *PLOS Computational Biology* **16**(11), 1–19 (2020). DOI 10.1371/journal.pcbi.1007575
76. Yu, X., Lu, L., Shen, J., Li, J., Xiao, W., Chen, Y.: A fractional-order SEIHDR model for COVID-19 with inter-city networked coupling effects. *Nonlinear Dynamics* **101**(3), 1717–1730 (2021). DOI 10.1007/s11071-020-05848-4
77. Zhang, S., Ponce, J., Zhang, Z., Lin, G., Karniadakis, G.: An integrated framework for building trustworthy data-driven epidemiological models: Application to the COVID-19 outbreak in New York City. *PLOS Computational Biology* **17**(9), 1–29 (2021). DOI 10.1371/journal.pcbi.1009334
78. Zhou, F., Yu, T., Du, R., Fan, G., Liu, Y., Liu, Z., Xiang, J., Wang, Y., Song, B., Gu, X., Guan, L., Wei, Y., Li, H., Wu, X., Xu, J., Tu, S., Zhang, Y., Chen, H., Cao, B.: Clinical course and risk factors for mortality of adult inpatients with COVID-19 in Wuhan, China: a retrospective cohort study. *The Lancet* **395**, 1054–1062 (2020). DOI 10.1016/S0140-6736(20)30566-3